Physics Working Group Report to the LBNE Reconfiguration Steering Committee

J. Appel[1], M. Bass[2], M. Bishai[3], S. Brice[1], E. Blucher[4], D. Cherdack[2], M. Diwan[3], B. Fleming[5], G. Gilchriese[6], Z. Isvan[3], B. Lundberg[1], W. Marciano[3], M. Messier[7], S. Parke[1], J. Reichanadter[8], G. Rameika[1], K. Scholberg[9], M. Shochet[4], J. Thomas[10], R. Wilson[2], E. Worcester[3], C. Young[8], G. Zeller[1],

[1] *Fermi National Accelerator Laboratory, Batavia, IL 60510, USA*
[2] *Department of Physics, Colorado State University, Fort Collins, CO 80523, USA*
[3] *Physics Department, Brookhaven National Laboratory, Upton, NY 11973, USA*
[4] *Department of Physics, University of Chicago, Chicago, IL 60637, USA*
[5] *Department of Physics, Yale University, New Haven, CT 06511, USA*
[6] *Physics Division, Lawrence Berkeley National Laboratory, Berkeley, CA 94720*
[7] *Department of Physics, Indiana University, Bloomington, IN 47405, USA*
[8] *Stanford Linear Accelerator Laboratory, Menlo Park, CA, USA*
[9] *Department of Physics, Duke University, Durham, NC 22708, USA*
[10] *Department of Physics and Astronomy, University College London, London, WC1E 6BT, UK*

(Dated: August 6, 2012)

This document summarizes the physics capabilities of a long-baseline neutrino experiment employing a liquid argon detector and fed by an intense neutrino beam from Fermilab. The locations considered for the detector are at the Homestake mine in South Dakota, the Soudan mine in Minnesota, and the Ash River, Minnesota site of the NOvA detector. The experimental reach as a function of detector mass is given for the neutrino mass hierarchy and CP violation phase as well as for proton decay, atmospheric neutrino studies, and neutrinos from supernova explosions.

CONTENTS

I. INTRODUCTION

Four years ago, HEPAP's P5 subpanel laid out a plan to maintain the United States as a world leader in high energy physics. Central to that plan was a world-class neutrino program utilizing a large underground detector in South Dakota fed by an intense neutrino source at Fermilab. Such an experiment would answer a number of important scientific questions. (1) Is there CP violation in the neutrino sector? The existence of matter this late in the universe's development requires CP violation, but the effect seen in the quark sector is much too small. The answer may be neutrino CP violation, and the proposed project would be the first to have the sensitivity needed to observe it. (2) Is the ordering of the neutrino mass states the same as that of the quarks, or is the order inverted? In addition to being an important question on its own, it has a major impact on our ability to determine whether the neutrino is its own antiparticle, which if true could reflect physics at energy scales much greater than those probed at the LHC. (3) Is the proton stable? The answer will provide clues to the unification of the forces of nature. (4) What physics and astrophysics can we learn from the neutrinos emitted in supernova explosions?

The proposed experiment would have addressed all of these questions, but its cost was found to be too large. We were asked to propose options for staging the program in a way that is both affordable and effective in doing the science. Here we provide the data needed to assess the reach of each option for the above scientific questions.

II. CONFIGURATIONS

During the committee's deliberations, the following detector configurations were considered.

Config. Number	Beam	Baseline	Off-axis angle	Location	Depth	Detector
1	NuMI LE	735km	0	Soudan	0	LAr 5, 10, 15, 34 kt
2	NuMI LE	735km	0	Soudan	2300ft	LAr 5, 10, 15, 34 kt
3	NuMI ME	810km	14mrad	Ash River	0	LAr 5, 10, 15, 34 kt
4	NuMI LE	810km	14mrad	Ash River	0	LAr 5, 10, 15, 34 kt
5	NuMI ME	810km	14mrad	Ash River	0	TASD 14 (NOνA), 40kt
7	LBNE LE	1300km	0	Homestake	0	LAr 5, 10, 15, 34 kt
8	LBNE LE	1300km	0	Homestake	4850ft	LAr 5, 10, 15, 34 kt

TABLE I. Configurations considered by the LBNE Reconfiguration Physics Working Group. NuMI LE (ME) refers to the low-energy (medium-energy) tunes of the existing NuMI beamline. LBNE LE is the low-energy tune of a new proposed beamline from Fermilab aimed at the Homestake Mine in South Dakota. LAr refers to a Liquid Argon Time-Projection Chamber, and TASD refers to a Totally Active Scintillator Detector.

III. LONG-BASELINE PHYSICS

Although the Standard Model of particle physics presents a remarkably accurate description of the elementary particles and their interactions, it is known that the current model is incomplete and that a more fundamental underlying theory must exist. Results from the last decade, that the three known types of neutrinos have nonzero mass, mix with one another and oscillate between generations, implies physics beyond the Standard Model [1].

The three-flavor-mixing scenario for neutrinos can be described by three mixing angles (θ_{12}, θ_{23} and θ_{13}) and one CP-violating phase (δ_{CP}). The probability for neutrino oscillation also depends on the difference in the squares of the neutrino masses, $\Delta m^2_{ij} = m^2_i - m^2_j$; three neutrinos implies two independent mass-squared differences (Δm^2_{21} and Δm^2_{32}).

The entire complement of neutrino experiments to date has measured five of the mixing parameters: three angles, θ_{12}, θ_{23}, and recently θ_{13}, and two mass differences, Δm^2_{21} and Δm^2_{32}. The sign of Δm^2_{21} is known, but not that of Δm^2_{32}. The value of θ_{13} has been determined to be much smaller than the other two mixing angles which are both large [2] [3], implying that mixing is qualitatively different in the neutrino and quark sectors. Table II summarizes the current values of the neutrino oscillation parameters obtained from a global fit to experimental data [4] and the measurement of θ_{13} from the Daya Bay reactor experiment [2]. A comparison to the equivalent mixing parameter values in the quark CKM matrix is also shown [5].

TABLE II. Best fit values of the neutrino mixing parameters in the PMNS matrix and comparison to the equivalent values in the CKM matrix

Parameter	Value (neutrino PMNS matrix)	Value (quark CKM matrix)
θ_{12}	$34 \pm 1^\circ$	$13.04 \pm 0.05^\circ$
θ_{23}	$43 \pm 4^\circ$	$2.38 \pm 0.06^\circ$
θ_{13}	$9 \pm 1^\circ$	$0.201 \pm 0.011^\circ$
Δm^2_{21}	$+(7.58 \pm 0.22) \times 10^{-5}$ eV^2	
$\lvert\Delta m^2_{32}\rvert$	$(2.35 \pm 0.12) \times 10^{-3}$ eV^2	$m_3 >> m_2$
δ_{CP}	no measurement	$67 \pm 5^\circ$

Assuming a constant matter density, the oscillation of $\nu_\mu \to \nu_e$ in the Earth for 3-generation mixing is described approximately by the following equation [6]

$$\begin{aligned} P(\nu_\mu \to \nu_e) \approx \sin^2\theta_{23} \frac{\sin^2 2\theta_{13}}{(\hat{A}-1)^2} \sin^2((\hat{A}-1)\Delta) \\ + \alpha \frac{\sin\delta_{CP}\cos\theta_{13}\sin 2\theta_{12}\sin 2\theta_{13}\sin 2\theta_{23}}{\hat{A}(1-\hat{A})} \sin(\Delta)\sin(\hat{A}\Delta)\sin((1-\hat{A})\Delta) \\ + \alpha \frac{\cos\delta_{CP}\cos\theta_{13}\sin 2\theta_{12}\sin 2\theta_{13}\sin 2\theta_{23}}{\hat{A}(1-\hat{A})} \cos(\Delta)\sin(\hat{A}\Delta)\sin((1-\hat{A})\Delta) \\ + \alpha^2 \frac{\cos^2\theta_{23}\sin^2 2\theta_{12}}{\hat{A}^2} \sin^2(\hat{A}\Delta) \end{aligned} \tag{1}$$

where $\alpha = \Delta m^2_{21}/\Delta m^2_{31}$, $\Delta = \Delta m^2_{31} L/4E$, $\hat{A} = 2VE/\Delta m^2_{31}$, $V = \sqrt{2} G_F n_e$, n_e is the density of electrons in the Earth, L is the distance between the neutrino source and the detector in km, and E is the neutrino energy in GeV. Recall that $\Delta m^2_{31} = \Delta m^2_{32} + \Delta m^2_{21}$. For antineutrinos, the second term in Equation 1 has the opposite sign, and the matter potential also has the opposite sign. The second term is proportional to the following CP violating quantity:

$$J_{CP} \equiv \sin\theta_{12}\sin\theta_{23}\sin\theta_{13}\cos\theta_{12}\cos\theta_{23}\cos^2\theta_{13}\sin\delta_{CP} \tag{2}$$

Equation 1 is an expansion in powers of α. The $\nu_\mu/\bar{\nu}_\mu \to \nu_e/\bar{\nu}_e$ oscillation probabilities from the approximate formula given in Equation 1 as a function of neutrino energy and baseline are shown in Figure 1 for both the normal mass hierarchy ($m_1 < m_2 < m_3$) and inverted mass hierarchy ($m_3 < m_1 < m_2$) . There are two very different oscillation scales driven by the two independent mass-squared differences (Δm^2_{21} and Δm^2_{32}). The maximal oscillation

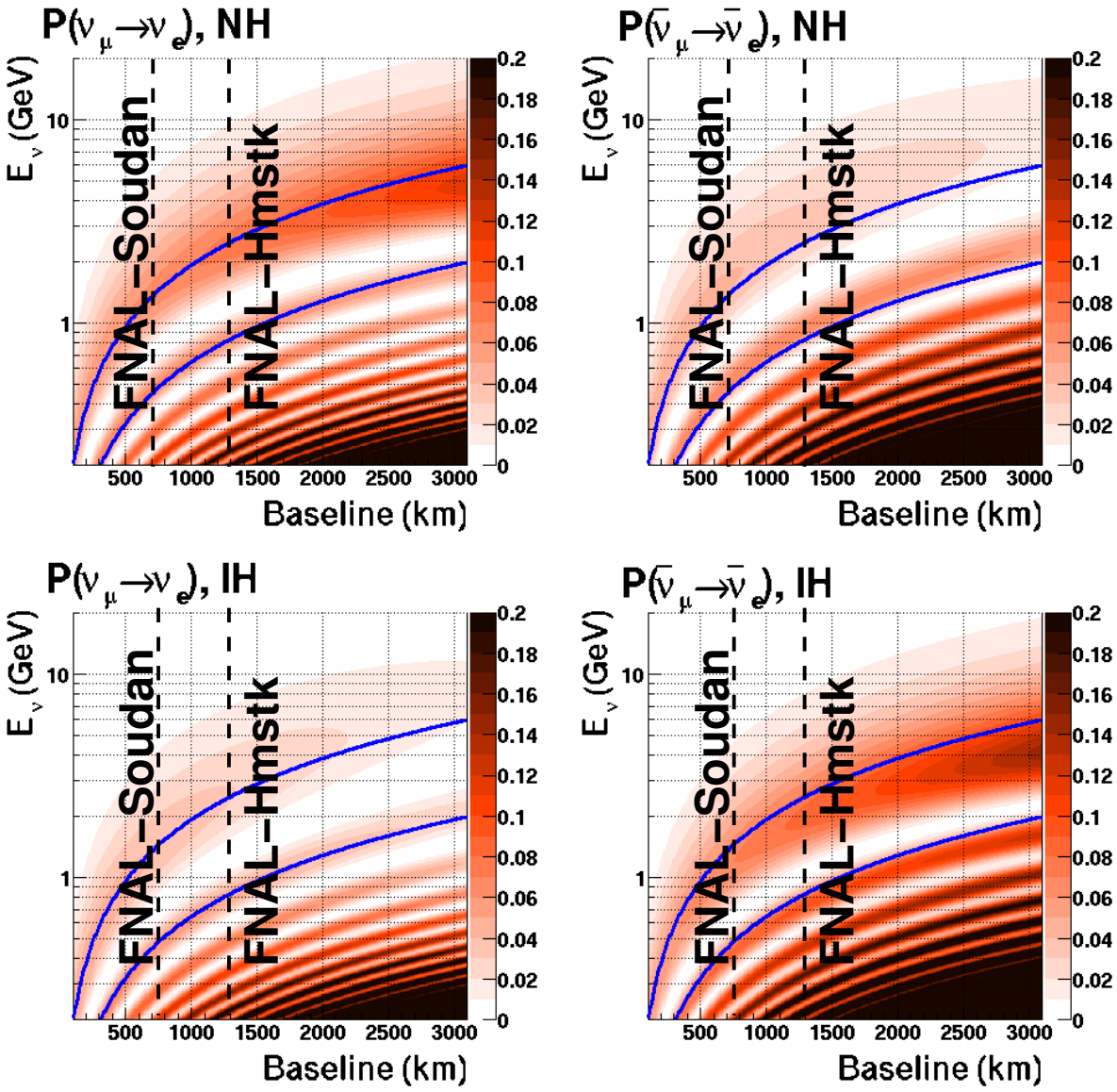

FIG. 1. The $\nu_\mu/\bar{\nu}_\mu \rightarrow \nu_e/\bar{\nu}_e$ oscillation probability vs neutrino energy and baseline with $\sin^2 2\theta_{13} = 0.1, \delta_{cp} = 0$ for normal hierarchy (top) and inverted hierarchy (bottom). The solid blue lines correspond to the locations of the 1^{st} and 2^{nd} oscillation maxima in vacuum.

probabilities occur at:

$$\begin{aligned} L/E_n^\nu \text{ (km/GeV)} &= (2n-1)\frac{\pi}{2}\frac{1}{(1.267 \times \Delta m^2 \text{ (eV}^2))} \\ &\approx (2n-1) \times 500 \text{ km/GeV for } \Delta m^2_{32} \text{ (atmospheric)} \\ &\approx (2n-1) \times 15,000 \text{ km/GeV for } \Delta m^2_{21} \text{ (solar)} \end{aligned} \tag{3}$$

where E_n^ν is the neutrino energy at the maximum of oscillation node n. The oscillations of $\nu_\mu \rightarrow \nu_e$ in long-baseline accelerator neutrino experiments are driven primarily by the atmospheric mass scale. The 1^{st} and 2^{nd} nodes are indicated as solid blue lines in Figure 1. The approximate formula given in Equation 1 is useful for understanding important features of the appearance probability shown in Figure 1:

1. The first three terms in the equation control the matter induced enhancement for normal mass ordering ($m_1 < m_2 < m_3$) or suppression for the inverted mass ordering ($m_3 < m_1 < m_2$) which dominates in the region of the

first oscillation node (largest E_ν).

2. The second and third terms control the sensitivity to CP and the value of δ_{cp} at the second oscillation node.

3. The last term controls the sensitivity to Δm^2_{21} and the solar oscillation parameters at the higher order oscillation nodes (largest L/E).

4. The first term (last term) is also proportional to $\sin^2\theta_{23}$ ($\cos^2\theta_{23}$), and therefore is sensitive to whether θ_{23} is above or below 45°.

The large non-zero value of θ_{13} indicates that measurement of the spectrum of oscillated $\nu_\mu \to \nu_e$ events over a large range of L/E in a single experiment will allow us access to all of the parameters in Equation 1 with good systematics control. Figure 1 demonstrates that the longer the experimental baseline the more oscillation nodes and the larger the range of L/E values are accessible.

The signature of CP violation is a difference in the probabilities for $\nu_\mu \to \nu_e$ and $\overline{\nu}_\mu \to \overline{\nu}_e$ transitions. The CP asymmetry $\mathcal{A}_{cp}$ is defined as

$$\mathcal{A}_{cp}(E_\nu) = \left[\frac{\mathrm{P}(\nu_\mu \to \nu_e) - \bar{\mathrm{P}}(\bar{\nu}_\mu \to \bar{\nu}_e)}{\mathrm{P}(\nu_\mu \to \nu_e) + \bar{\mathrm{P}}(\bar{\nu}_\mu \to \bar{\nu}_e)}\right] \tag{4}$$

The observed asymmetry $\mathcal{A}$ is a combination of both the CP asymmetry and the asymmetry due to the matter effect. Figure 2 shows the maximal possible CP asymmetry in vacuum ($\delta_{cp} = -\pi/2$) and the asymmetry from the matter effect alone as a function of energy and baseline. The CP asymmetry arising from non-zero/π values of δ_{cp} is dominant in the L/E regions of the secondary oscillation nodes and is constant as a function of baseline, whereas the asymmetry due to the matter effect dominates the L/E region of the first oscillation node and increases with longer baselines.

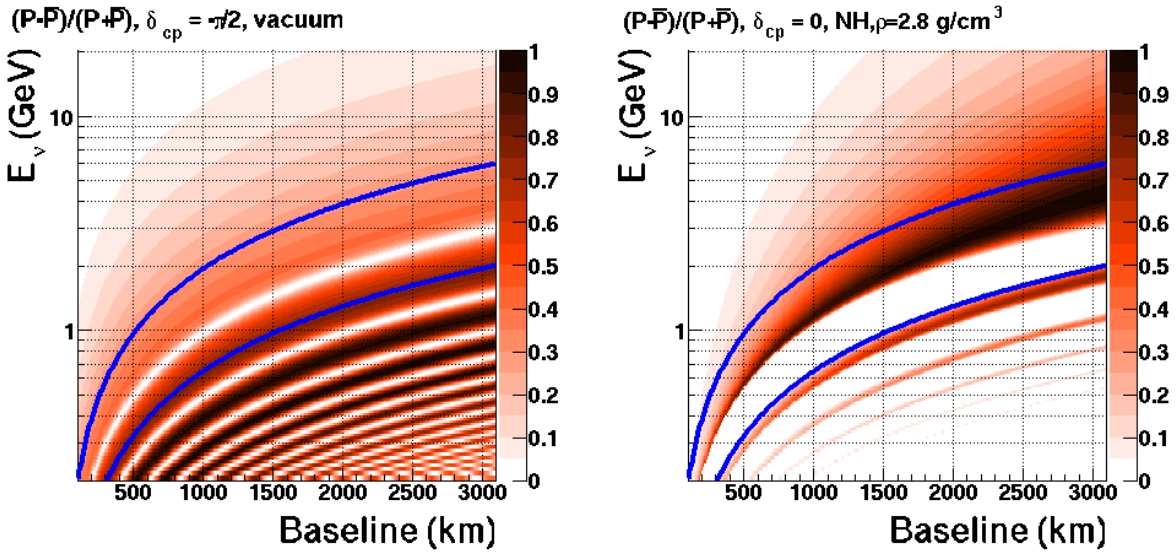

FIG. 2. The asymmetry, $\mathcal{A}_{cp}$, for maximal CP violation in vacuum (left) and arising from the matter effect only (right) as a function of energy and baseline. An average earth density of $\rho = 2.8$ g/cm^3 is assumed for the matter effect.

Observations of $\nu_\mu \to \nu_e$ oscillations of a beam (composed initially of muon neutrinos, ν_μ) over a long baseline and a wide range of neutrino energies are thus the key to unambiguously determining the mass hierarchy (the sign of Δm^2_{32}), and the unknown CP-violating phase δ_{cp}. The study of $\nu_\mu \to \nu_e$ oscillations can also help determine the θ_{23} quadrant since the first and fourth terms in Equation 1 are proportional to $\sin^2\theta_{23}$ and $\cos^2\theta_{23}$ respectively.

The study of the disappearance of ν_μ probes $\sin^2 2\theta_{23}$ and $|\Delta m^2_{32}|$. Non-standard physics can manifest itself in differences observed in higher precision measurements of ν_μ and $\bar{\nu}_\mu$ disappearance over long baselines and in observing deviations from the 3-flavor model in $\nu_\mu \to \nu_e$ oscillations. The precision with which we know the current set of neutrino oscillation parameters ensures that the compelling physics program outlined is feasible with the combination of a long-baseline, very large detector mass, and a wide-band beam with beam energies matched to the baseline as summarized in Equation 3.

The primary scientific goals of the next generation of long-baseline neutrino experiments is to carry out the most precise measurements of the three-flavor neutrino-oscillation parameters over a very long baseline and a wide range of neutrino energies, in particular, the CP-violating phase in the three-flavor framework. Precision measurements of the 3-flavor neutrino oscillation parameters will also enable the search for new physics that manifests itself as deviations from the expected three-flavor neutrino-oscillation model.

A. The Neutrino Beams

The three beam configurations under consideration are the 1) LBNE beamline in the low energy configuration on-axis with a detector at Homestake Mine (1300km), 2) the NuMI beamline in the low energy configuration with a detector on-axis at Soudan Mine (735km), and 3) the NuMI beamline in the medium energy configuration with a detector 14mrad off-axis at Ash River (810km). The neutrino beamline parameters used in the GEANT3 simulation for each of these options are summarized in Table III.

TABLE III. The NuMI and LBNE neutrino beam configurations used in this study

	LBNE LE [a]	NuMI LE	NuMI ME
Primary beam	120 GeV p^+	120 GeV p^+	120 GeV p^+
Beam power	708 kW	708 kW	708 kW
POT/yr	6.0×10^{20}	6.0×10^{20}	6.0×10^{20}
Target material	graphite	graphite	graphite
Target cross-section	circular d=1.2cm	rectangular w=0.64cm h=2cm	rectangular w=0.64cm h=2cm
Target length	2 interaction lengths	2 interaction lengths	2 interaction lengths
Focusing horns (1/2)	NuMI, 250kA	NuMI, 185 kA	NuMI, 200 kA
Horn separation	6m	10m	23m
Target-Horn 1 distance	30cm	45cm	135 cm
Decay pipe	4m diameter, 280m long	2m diameter, 677m long	2m diameter, 677m long
	Evacuated/He filled	He filled	He filled

[a] The LBNE decay pipe in the conceptual design has a length between 200 and 250m and is filled with air.

All the beamline designs considered can be operated in neutrino or anti-neutrino mode by reversing the horn current to charge select positive or negative hadrons. The ν_μ and $\bar{\nu}_\mu$ charged current spectra at each candidate far detector location are shown in Figure 3 with the ν_e appearance probability curves overlaid. We note that there is a small ν_e beam contaminant of order 1% from μ and Ke3 decays. There is also a wrong-sign ν_μ contaminant in each beam ($\approx 10\%$) from decays of unfocused hadrons. The numbers of expected neutrino and anti-neutrino events at the three potential sites are given in Table IV.

TABLE IV. Number of events per 100kt.MW.yrs (1 MW.yr= 1×10^{21} protons-on-target) for $\sin^2 2\theta_{13} = 0.1, \delta_{cp} = 0$, normal mass ordering in the visible energy range 0.5 to 20 GeV. CC refers to charged-current interactions, and NC to neutral-current interactions. The ν_μ CC unosc. rates are the estimated event rates without oscillations, the ν_μ CC osc. rates are the event rates with $\nu_\mu \to \nu_\mu$ oscillations. ν_e beam refers to the ν_e contaminant in the beam. The first 6 columns of numbers are for neutrino beams, and the last 6 columns are for anti-neutrino beams.

Expt	ν_μ CC Unosc.	ν_μ CC Osc.	ν_μ NC	ν_e beam CC	$\nu_\mu \to \nu_e$ CC	$\nu_\mu \to \nu_\tau$ CC	$\bar{\nu}_\mu$ CC Unosc.	$\bar{\nu}_\mu$ CC Osc.	$\bar{\nu}_\mu$ NC	$\bar{\nu}_e$ beam CC	$\bar{\nu}_\mu \to \bar{\nu}_e$ CC	$\bar{\nu}_\mu \to \bar{\nu}_\tau$ CC
Ash River 810km	18K	7.3K	3.6K	330	710	38	7.1K	2.5K	1.8K	110	210	
Soudan 735km	73K	49K	15K	820	1500	166	27K	18K	13K	285	495	54
Hmstk 1300km	29K	11K	5.0K	280	1300	130	11K	3.8K	3.0K	86	273	46

B. The LAr-TPC Neutrino Detector

Neutrino events detected in experiments like LBNE are often categorized according to the particle mediating the interaction. The term (used below, and throughout this document) "neutral current process" (NC) refers to an interaction which is mediated by the neutral boson Z^0. Similarly, a "charged current" (CC) interaction involves a postive or negative charged W boson. The flavor of a neutrino in a CC interaction is tagged by the flavor of the emitted lepton: e, μ, or τ tag for a ν_e, ν_μ, or ν_τ interaction respectively. A "quasi-elastic" (QE) event is a CC event in which

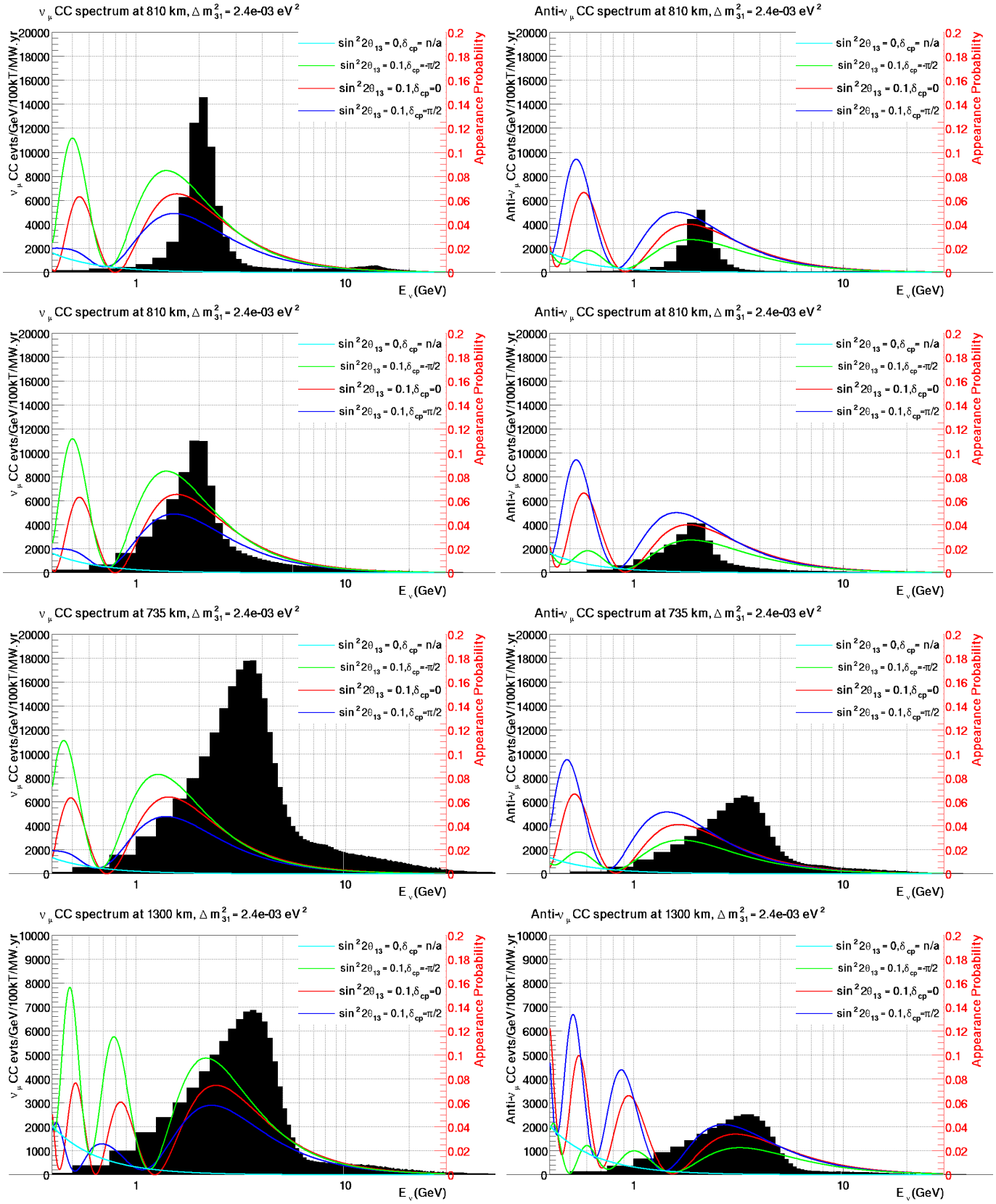

FIG. 3. The un-oscillated ν_μ CC spectra at the 3 candidate locations (black histograms) with the ν_e appearance probability curves for $\sin^2 2\theta_{13} = 0.1, \delta_{cp} = 0$ (red) $\pi/2$ (blue) $-\pi/2$ (green) with normal mass ordering. The curve in cyan shows the contribution from the fourth term of Equation 1 which is driven by the solar oscillation and is independent of $\sin^2 2\theta_{13}$ and δ_{cp}. The figures are from top to bottom: NuMI ME at Ash River, NuMI LE at Ash River, NuMI LE at Soudan, and the LBNE beam at Homestake. The left set of figures is for neutrino running and the right set of figures is for anti-neutrino running.

the scattering of the neutrino is almost elastic with only a charged lepton and a nucleon or nucleons emerging from the target nucleus. The charged lepton in QE events carries most of the energy of the neutrino, and as a result, QE interactions have the best neutrino-energy resolution. Final State Interactions (FSI) inside the nucleus will alter the expected nucleon types and spectrum, and a measurement of this effect is an important goal of the Near Detector. CC and NC interactions of neutrinos with energies > 1 GeV are inelastic and the target nucleus disintegrates producing multiple hadrons.

The cross-section of $\nu/\bar{\nu}$ CC and NC interactions [7] for different event categories is shown in Figure 4.

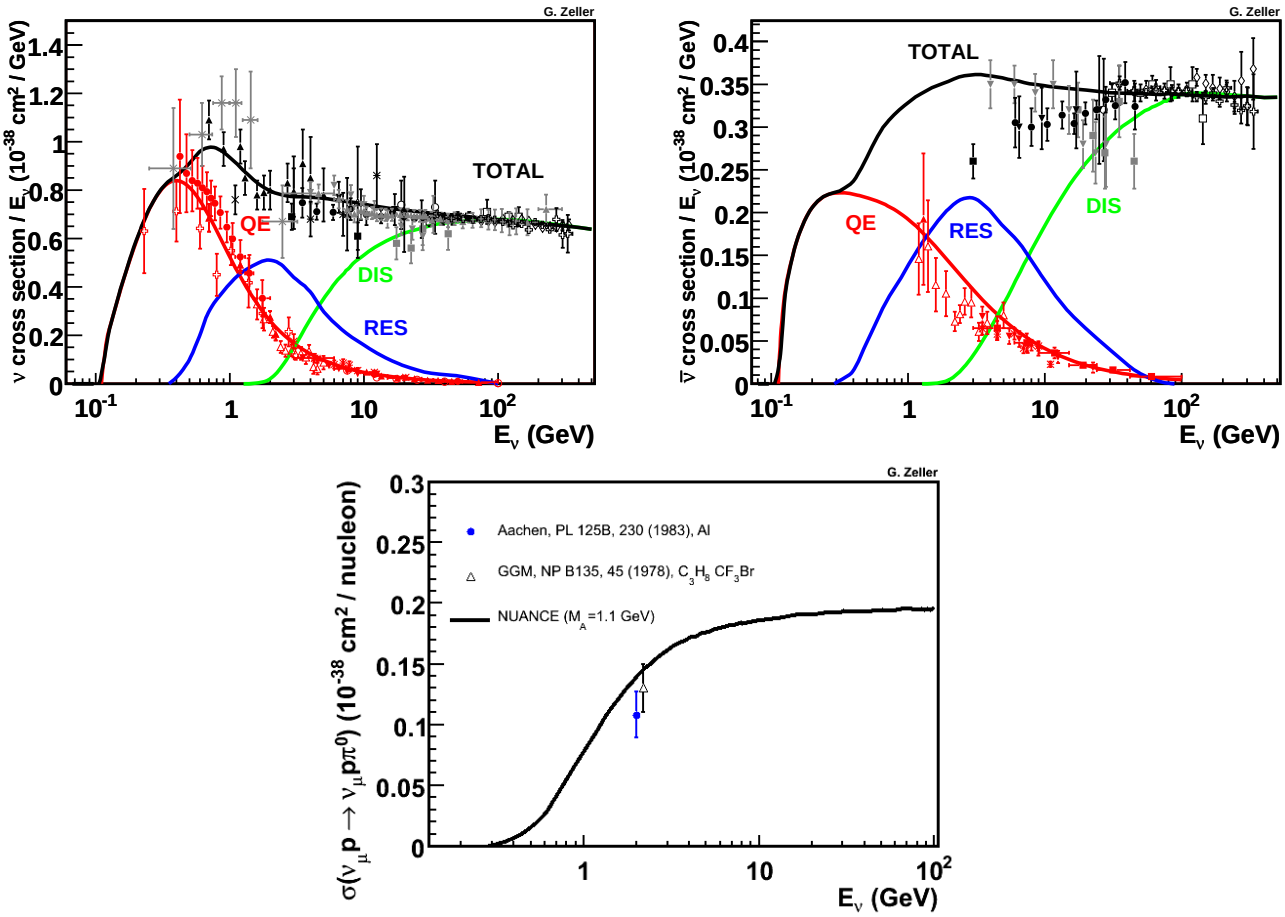

FIG. 4. Neutrino charged-current interaction cross-sections divided by neutrino energy for neutrinos (top-left), and anti-neutrinos (top-right) for an isoscalar target plotted as a function of neutrino energy. Also shown are the contributions to the total cross section from quasi-elastic scattering (red), resonance production (blue), and deep inelastic scattering (green) processes. Example predictions for each are provided by the NUANCE generator [8]. Note that the quasi-elastic scattering data and predictions have been averaged over neutron and proton targets and hence have been divided by a factor of 2 for the purposes of this plot. On the bottom are existing measurements of the cross section for the NC process, $\nu_\mu\, p \to \nu_\mu\, p\, \pi^0$, as a function of neutrino energy. The Gargamelle measurement comes from a more recent re-analysis of this data [9]. Also shown is the prediction from [8]. All three Plots are from [7].

A substantial component of the background for ν_e CC interactions comes from NC interactions where a π^0 is produced. The π^0 decays to two γs which shower electromagnetically and fake electrons. NC interactions where a charged pion is produced are also the predominant background for ν_μ CC interactions where the pion fakes a muon. Therefore to study neutrino flavor oscillations with high precision, the LBNE Far Detector has to have high efficiency and high purity $e/\mu/\gamma$ and $\pi/K/p$ separation.

A massive liquid argon TPC (LArTPC) has been chosen as the Far Detector technology for the LBNE project [10]. TPCs are the detectors of choice for low-rate, large-volume, high-precision particle physics experiments due to their excellent 3D position resolutions and particle identification in large volumes. In addition to detailed event topologies and measurements of particle kinematics, dE/dx measurements allow TPCs to unambiguously distinguish electrons, muons, photons, kaons, pions and protons over a wide range of energies. Examples of how event topologies can be

used to identify ν_e/ν_μ CC and ν NC events in a LAr-TPC are shown in Figure 5. The expected signal efficiencies and

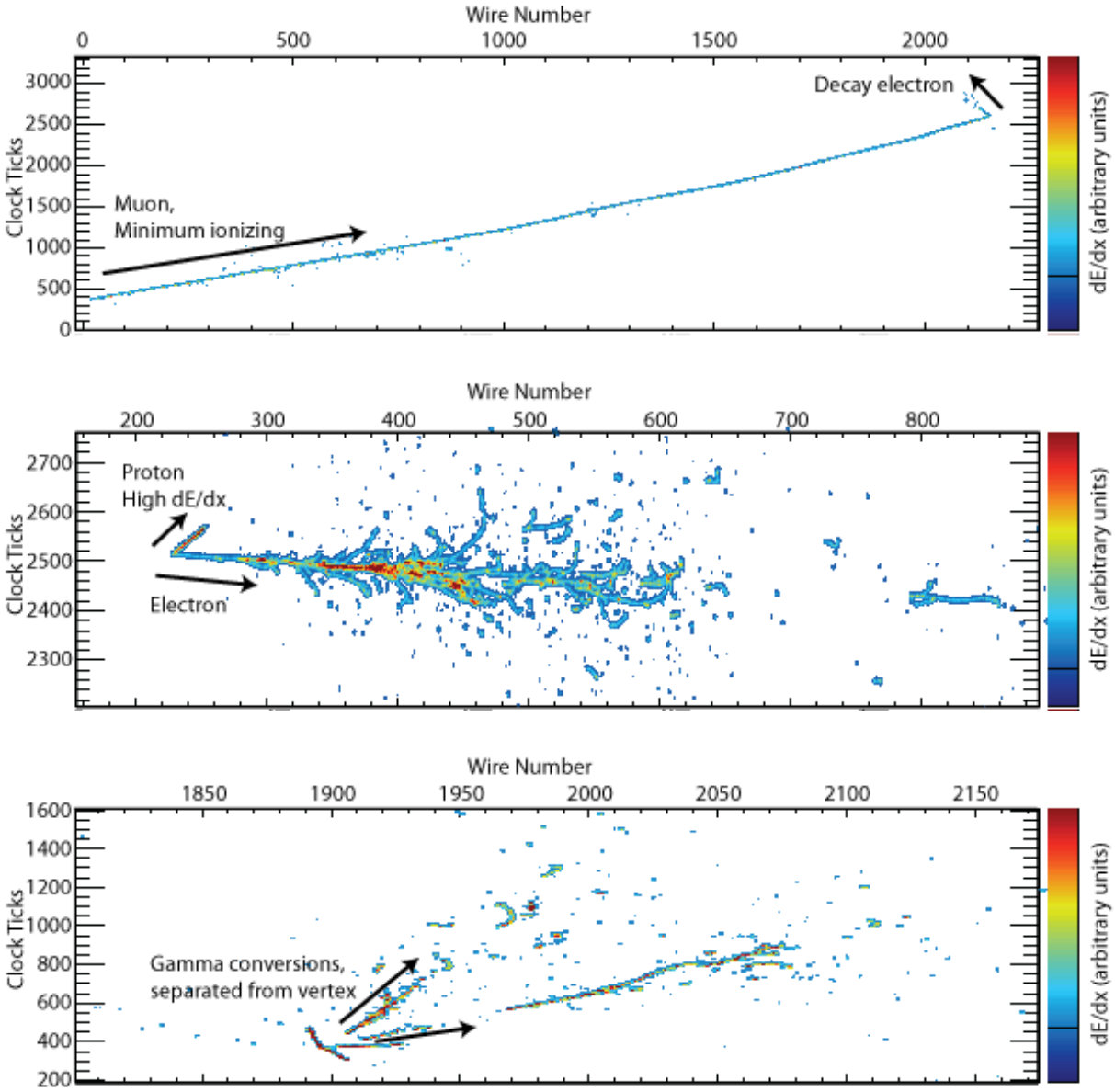

FIG. 5. Examples of neutrino beam interactions in an LArTPC obtained from a GEANT4 simulation [11]. A CC ν_μ interaction with a stopped μ followed by a decay Michel electron (top), a QE ν_e interaction with a single electron and a proton (middle), an NC interaction which produced a π^0 that then decayed into two γ's with separate conversion vertices (bottom).

background mis-identification rates as well as the energy resolution for different event types are summarized in Table V. The performance parameters were derived from several visual scan studies carried out using GEANT4 simulation of LAr-TPC as shown in Figure 5, from studies of the ICARUS detector performance [12–14] and from automated reconstruction used in the LAr detector proposal for a detector at a 2km baseline in the T2K experiment [16].

The performance parameters summarized in Table V were implemented into the GLoBES software package [17]. The expected spectrum of ν_e or $\overline{\nu}_e$ oscillation events from a parameterized implementation of a 34-kton LArTPC running with 5 years of neutrino and 5 years of anti-neutrino 700kW beam assuming $\sin^2(2\theta_{13}) = 0.1$ and normal mass ordering is shown in Figure 6. The expected spectrum of ν_μ or $\overline{\nu}_\mu$ oscillation events is shown in Figure 7.

The GLoBES experimental assumptions for the NOνA and T2K experiments used in this study were obtained from references [18, 19] and [20–22] respectively. The assumptions for the NOνA experiment are summarized in Table VI.

Operating a large liquid argon detector on the Earth's surface is currently under study by the LBNE collaboration.

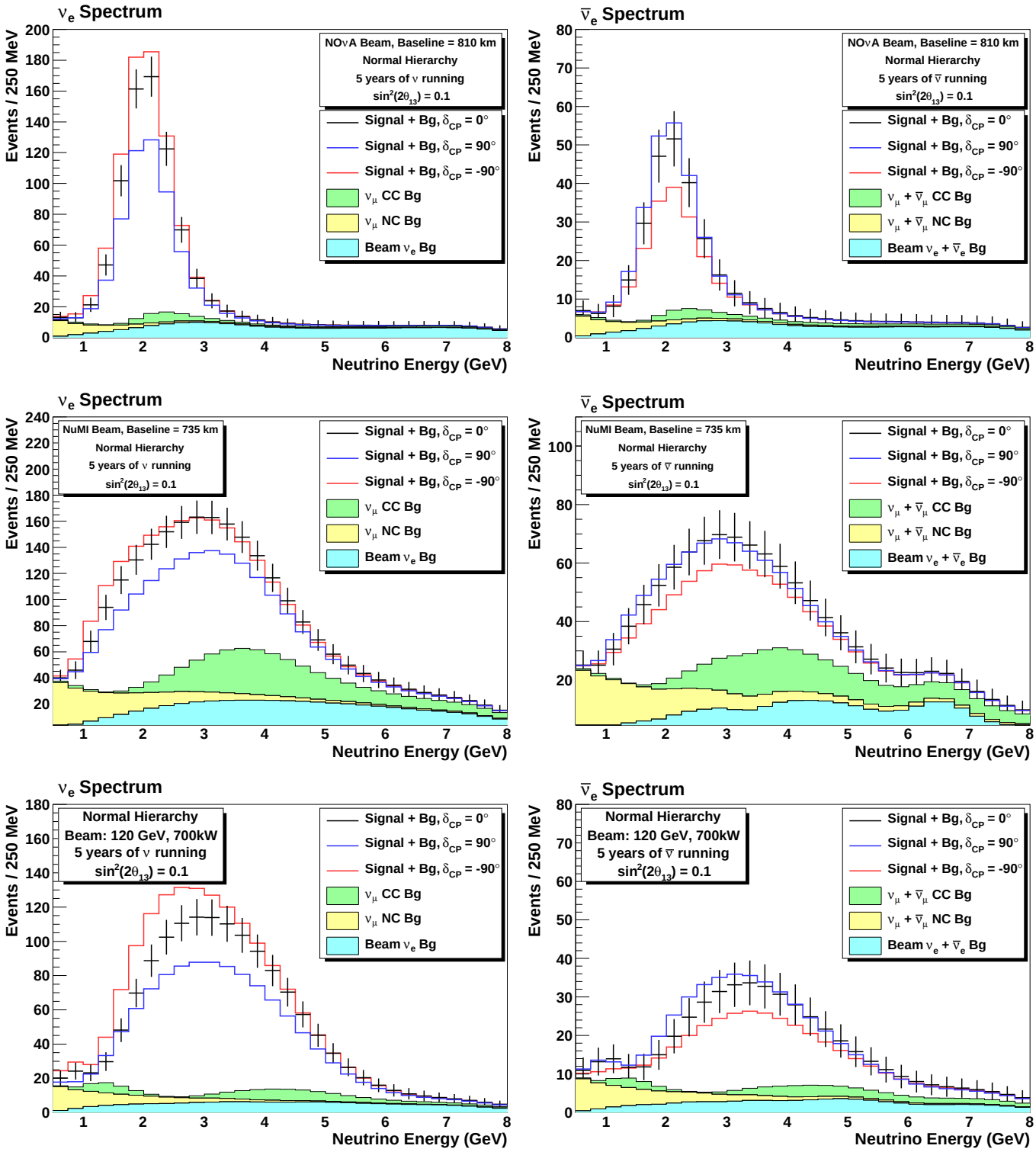

FIG. 6. The expected spectrum of ν_e or $\overline{\nu}_e$ oscillation events in a 34-kton LArTPC for 5 years of neutrino (left) and anti-neutrino (right) running with a 700 kW beam assuming $\sin^2(2\theta_{13}) = 0.1$ and normal mass ordering. Backgrounds from intrinsic beam ν_e (cyan), ν_μ NC (yellow), and ν_μ CC (green) are displayed as stacked histograms. The points with error bars are the expected total event rate for $\delta_{cp} = 0$; the red (blue) histogram is the total expected event rate with $\delta_{cp} = -\pi/2(+\pi/2)$. The figures are from top to bottom: NuMI ME at Ash River, NuMI LE at Soudan and the LBNE beam at Homestake.

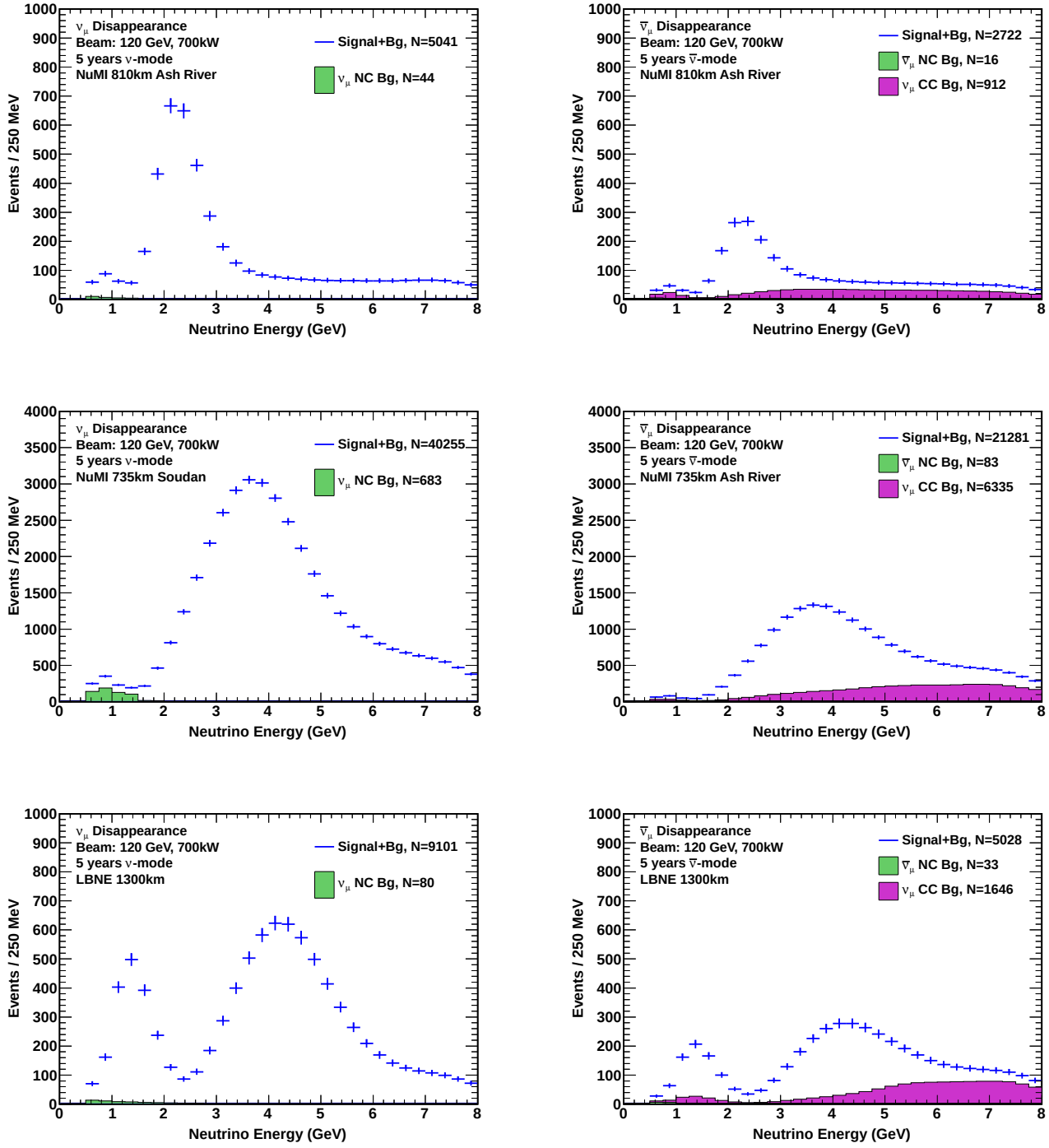

FIG. 7. The expected spectrum of ν_μ or $\overline{\nu}_\mu$ oscillation events in a 34-kton LArTPC for 5 years of neutrino (left) and anti-neutrino (right) running with a 700 kW beam. The points with error bars are the expected total event rate for $\Delta^2 m_{32} = 2.35$ and $\sin^2 2\theta_{23} = 0.1$. Backgrounds from NC and the wrong sign ν are displayed. The figures are from top to bottom: NuMI ME at Ash River, NuMI LE at Soudan and the LBNE beam at Homestake.

TABLE V. Estimated range of the LAr-TPC detector performance parameters for the primary oscillation physics. The expected range of signal efficiencies, background levels, and resolutions from various studies (middle column) and the value chosen for the baseline LBNE neutrino-oscillation sensitivity calculations (right column) are shown. * For atmospheric neutrinos this is the mis-identification rate for < 2 GeV events, the mis-identification rate is taken to be 0 for > 2 GeV.

Parameter	**Range of Values**	**Value Used for LBNE Sensitivities**
Identification of ν_e CC events		
ν_e CC efficiency	70-95%	80%
ν_μ NC mis-identification rate	0.4-2.0%	1%
ν_μ CC mis-identification rate	0.5-2.0%	1%
Other background	0%	0%
Signal normalization error	1-5%	1%
Background normalization error	2-10%	5%
Identification of ν_μ CC events		
ν_μ CC efficiency	80-95%	85%
ν_μ NC mis-identification rate	0.5-10%	0.5%
Other background	0%	0%
Signal normalization error	1-5%	5%
Background normalization error	2-10%	10%
Identification of ν NC events		
ν NC efficiency	70-95%	90%
ν_μ CC mis-identification rate	2-10%	10% *
ν_e CC mis-identification rate	1-10%	10% *
Other background	0%	0%
Signal normalization error	1-5%	
Background normalization error	2-10%	
Neutrino energy resolutions		
ν_e CC energy resolution	$15\%/\sqrt{E(GeV)}$	$15\%/\sqrt{E(GeV)}$
ν_μ CC energy resolution	$20\%/\sqrt{E(GeV)}$	$20\%/\sqrt{E(GeV)}$
E_{ν_e} scale uncertainty		
E_{ν_μ} scale uncertainty	1-5%	2%

Initial results on muon-induced background are presented in a supporting document on the LBNE Reconfiguration website [23]. GEANT simulation indicates that there are cuts which reduce the background to a few events per year while retaining high signal efficiency. A system of photon detectors, which would improve the time resolution of the experiment, would further reduce the background to less than 1 event per year.

The need for a near detector is analyzed in a supporting document [24]. A full near detector, with a design similar to that of the far detector, will be needed for later phases of LBNE when high statistics allow a variety of searches for physics beyond the 3×3 ν-matrix model. However for phase-1 and its primary goals of determining the neutrino mass hierarchy and measuring the CP phase, a simpler and less costly near detector should suffice. This could include a magnetized detector to measure the muon neutrino and anti-neutrino spectra and an existing liquid argon TPC on the surface to detect off-axis neutrinos and measure the π^0 production rate.

C. Mass Hierarchy and CP Violation Sensitivity

The long-baseline physics capabilities of a LAr-TPC far detector in the proposed LBNE project is described in detail in [25]. In these sections we will focus on the comparison of physics capabilities of a LAr-TPC at Homestake with a LAr-TPC detector placed in the NuMI beam at the Soudan and Ash River locations.

We use the GLoBES software package to estimate the significance, σ, with which we can 1) exclude the opposite mass hierarchy, and 2) exclude $\delta_{cp} = 0$ or π (CP violation). A True appearance event spectrum is generated for a given value of $\delta_{cp}, sign(\Delta m^2_{31})$ as shown in Figure 6. A minimum χ^2 fit is performed to the given hypothesis. The minimization accounts for the correlations between the different mixing parameters which are included with Gaussian constraints based on the best fit uncertainties as summarized in Table II. The disappearance experiment as shown in Figure 7 is included in the minimization and helps to constrain the atmospheric parameters. The normalization uncertainties on the signal and background listed in Table V are included as nuisance parameters. θ_{13} is constrained

TABLE VI. Detector efficiencies and background rejection assumptions for NOνA used in sensitivity calculations.

Parameter	**Value Used (NOνA)**
Identification of ν_e CC events	
ν_e CC efficiency	26% (ν) 41% ($\bar{\nu}$)
ν_μ NC mis-identification rate	0.28% (ν) 0.88% ($\bar{\nu}$)
ν_μ CC mis-identification rate	0.13%
Other background	0%
Signal normalization error	5%
Background normalization error	10%
Identification of ν_μ CC events	
ν_μ CC efficiency	100% (QE only)
ν_μ NC mis-identification rate	0.1%
Other background	0%
Signal normalization error	2%
Background normalization error	10%

using the projected accuracy expected from the final run of the current reactor experiments (3%). When estimating the sensitivity to the mass hierarchy, the χ^2 minimization is performed over all values of δ_{cp}. The opposite mass hierarchy is included in the minimization when estimating the χ^2 to determine whether CP is violated ($\delta_{cp} \neq 0$ or π). The significance with which we can exclude the opposite mass hierarchy and determine whether $\delta_{cp} \neq 0$ or π is defined as $\sigma = \sqrt{\chi^2}$. The significance as a function of δ_{cp} is shown in Figure 8 for three different LAr-TPC masses, 10, 15, and 34 kt placed at Soudan, Ash River, and Homstake. No constraints from other experiments are included.

The relatively poor performance for $\delta_{cp} > 0$ for the Minnesota sites is due to the inability to determine the mass hierarchy with those experiments alone. Sensitivity to the hierarchy depends strongly on the baseline and the energy spread of the beam. The very long-baseline to Homestake makes the problem easier. For the shorter baseline to the Minnesota sites, it is more difficult, especially for $\delta_{cp} > 0$ where the CP and matter effects are of opposite sign. The situation is significantly improved if results from the T2K experiment in Japan are included in a global analysis. T2K's short baseline greatly reduces the matter effect. This allows the two effects to be separated in the global analysis. However it must be remembered that success depends on understanding in detail the systematics of several experiments and their correlations. The significance of the hierarchy measurement when results from a 15 kt LAr-TPC are combined with the NOνA, and T2K experiments is shown in Figure 9. For the combinations with a LAr-TPC at the Minnesota site the NOνA experiment is assumed to run concurrently for a total of 16 yrs. We use a 6 year run when combining NOνA results with the experiment at Homestake. A total of 5×10^{21} integrated protons on target is assumed for the T2K experiment. The significance with which CP violation is resolved with a LAr-TPC at Ash River Soudan, and Homestake when combined with NOνA and T2K running is also shown in Figure 9. The opposite mass hierarchy is considered when estimating the CP violation significance with different experimental combinations.

In Figure 10, the significance with which CP violation is resolved for 50% of δ_{cp} values as a function of exposure in kt.yrs with a LAr-TPC at Homestake , Ash River, and Soudan is shown. The sensitivity of the NOνA experiment (estimated using the GLoBES package) with increasing exposure is also displayed for reference.

D. Precision Measurement of Neutrino Mixing Parameters

One of the primary scientific goals of the LBNE experiment is to carry out the most precise measurements of the three-flavor neutrino-oscillation parameters. The precision with which the values of δ_{cp} and $\sin^2 2\theta_{13}$ can be determined in the $\nu_\mu \rightarrow \nu_e$ appearance mode as a function of exposure in yrs and mass is shown in Figures 11, and 12 respectively. It is to be noted that for measurements of δ_{cp}, the resolution is limited by the degeneracy between δ_{cp} and other mixing parameters such as θ_{13}, θ_{23} and the mass ordering. External constraints on θ_{13} from the reactor experiments improves the δ_{cp} resolution from the NuMI options for values of δ_{cp} in the vicinity of $|\pi/2|$ (maximal CP violation). LBNE-Homestake provides enough internal constraints on the other mixing parameters and the mass ordering that the impact of degeneracies is much less pronounced. Its to be noted that Figures 11 and 12 assume the mass ordering is resolved for all values of δ_{cp}.

The precision with which the values of $\sin^2 2\theta_{23}$ and $|\Delta m^2_{31}|$ can be determined from a joint fit to the $\nu_\mu \rightarrow \nu_\mu$ disappearance mode and $\nu_\mu \rightarrow \nu_e$ appearance mode as a function of exposure in years and mass is shown in Figures

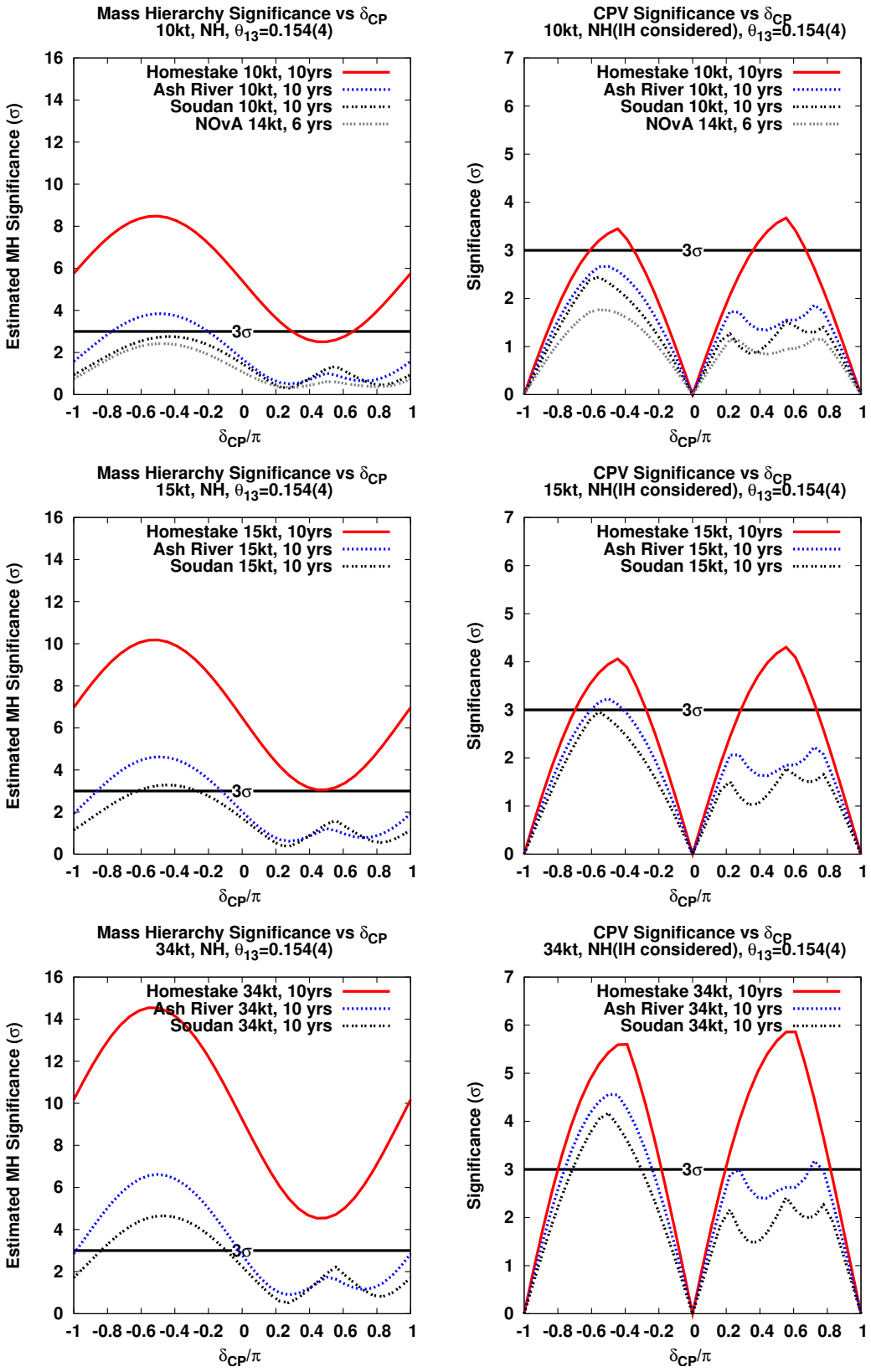

FIG. 8. The significance with which the mass ordering (left) and CP violation ($\delta_{cp} \neq 0, \pi$) is resolved (right) with a LAr-TPC at Homestake (red), Ash River (blue-dashed), Soudan (black-dashed) as a function of the unknown CP violating phase δ_{cp}. The sensitivity of the NOνA experiment with 14 kt of a totally active liquid scintillator detector (TASD) at Ash River is shown in gray. The plots are from top to bottom: 10kt, 15kt and 34kt. The significance is calculated using the current constraints on the mixing parameters from the global fit as shown in Table II. θ_{13} is constrained using the projected accuracy expected from the current reactor experiments (3%). The opposite mass hierarchy is considered when calculating the CP violation significance. There is no T2K constraint on the mass hierarchy. An exposure of 5 yrs neutrino running combined with 5 yrs of anti-neutrino running in a 700kW beam is assumed. The NuMI LE beam is used at Soudan and at Ash River.

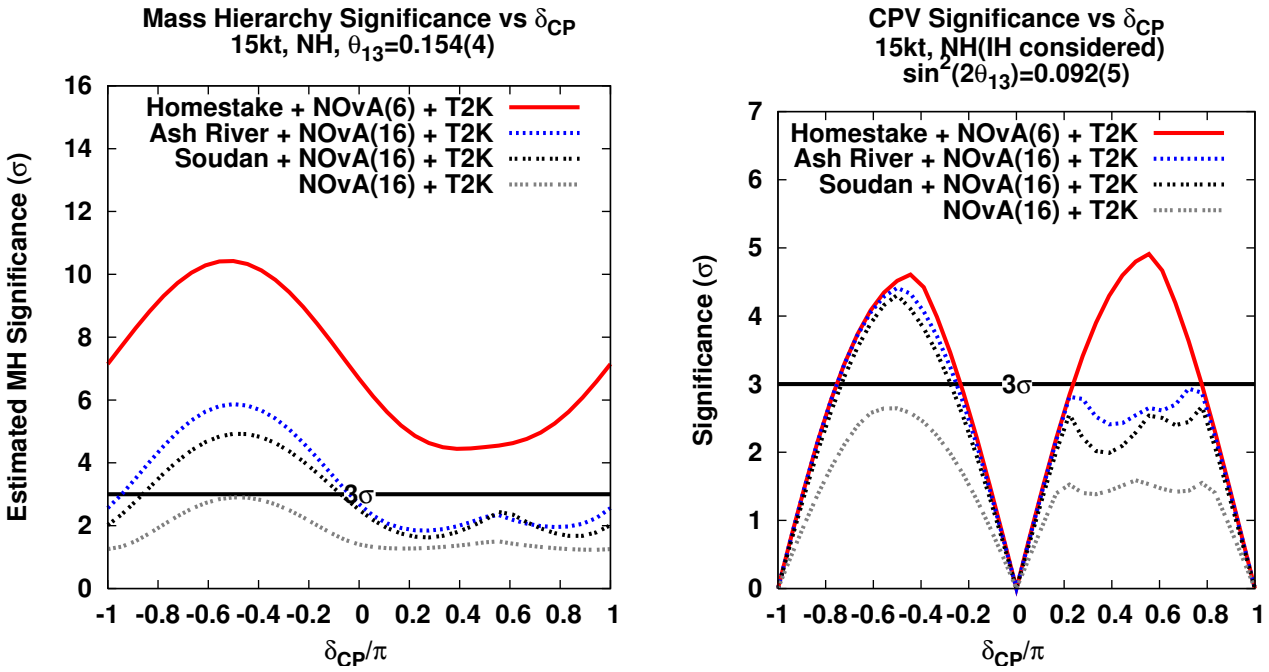

FIG. 9. The significance with which the mass ordering (left) and CP violation (right) is resolved when a 15 kt LAr-TPC at Homestake (red), Ash River (blue-dashed), Soudan (black-dashed) is combined with NOνA running with the ME beam for 3+3 years (I), the LE beam for 5+5 yrs (II) and T2K (5×10^{21} protons-on-target). The significance just from NoVA I+II combined with T2K is shown as gray-dashed line.

13, and 14 respectively. The measurements from neutrino and anti-neutrino running in the ratio 1:1 are combined. The current best measurements of $|\Delta m^2_{32}|$ for neutrinos and anti-neutrinos measured separately are from the MINOS experiment [26] utilizing only the signal in the disappearance mode.

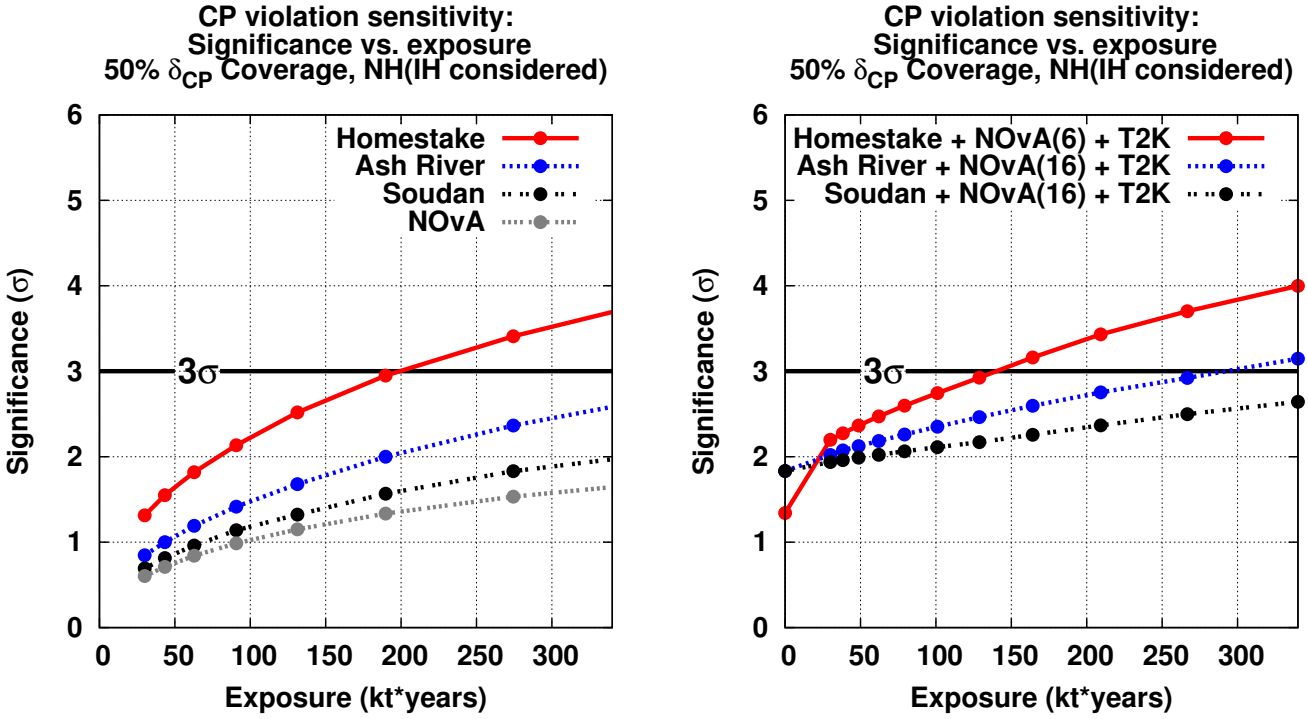

FIG. 10. The significance with which CP violation is resolved for 50% of δ_{cp} values as a function of exposure in kt.yrs with a LAr-TPC at Homestake (red), Ash River (blue-dashed), Soudan (black-dashed). The sensitivity of the NOνA experiment with a totally active liquid scintillator detector (TASD) at Ash River is shown in gray. The results are for neutrino and anti-neutrino running in the ratio 1:1 with a 700kW beam assuming 6.0×10^{20} protons-on-target per year. The NuMI LE beam is used at Soudan and Ash River. The measurements include a constraint on $\theta_{13} = 0.154 \pm 0.005$ and take into account all correlations with the other mixing parameters which are constrained using the current best estimate of the uncertainties as summarized in [4]. Both mass hierarchies are considered when estimating the sensitivities to CP violation. The figure on the left is the sensitivity achieved by each individual experiment. The figure on the right shows the sensitivities achieved combining the LAr-TPC with NOνA and T2K (5×10^{21} integrated protons-on-target). For the Homestake option, it is assumed NOνA will run for 6 yrs at 700kW; for the Minnesota sites it is assumed NOνA will run for 16 yrs.

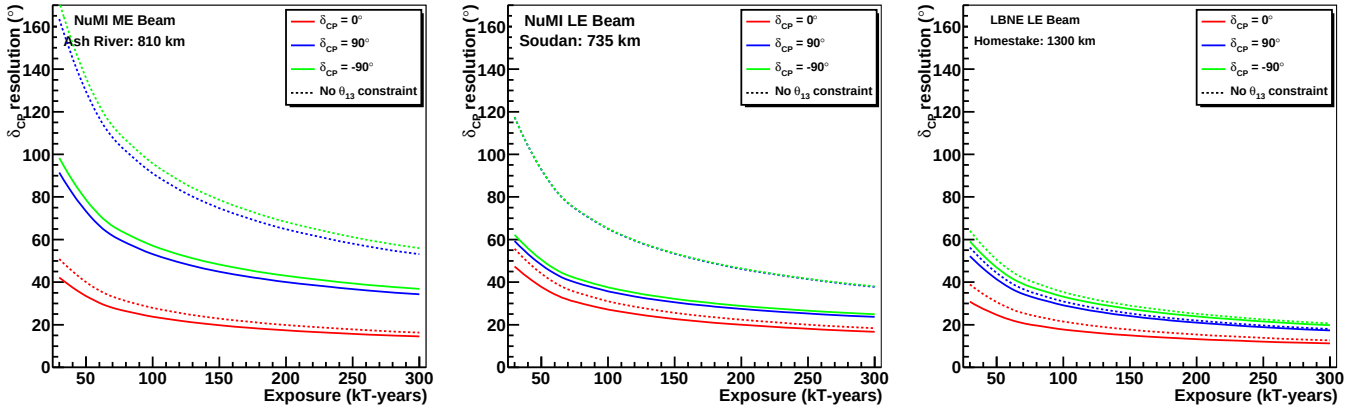

FIG. 11. The 1σ resolution on the measurement of δ_{cp} as a function of exposure in kt.yrs for $\delta_{cp} = 0$ (red), $\pi/2$ (blue), $-\pi/2$ (green). The exposure in yrs is assumed to be $1/2$ ν and $1/2$ $\bar{\nu}$ running at 700kW. The solid lines include the tight external constraint on $\theta_{13} = 0.154 \pm 0.005$. The dashed lines are without any external constraints on θ_{13}. The plots from left to right are for Ash River, Soudan, and Homestake. The measurements assume $\sin^2 2\theta_{13} = 0.092$ and normal hierarchy. **The mass hierarchy is assumed to be known.**

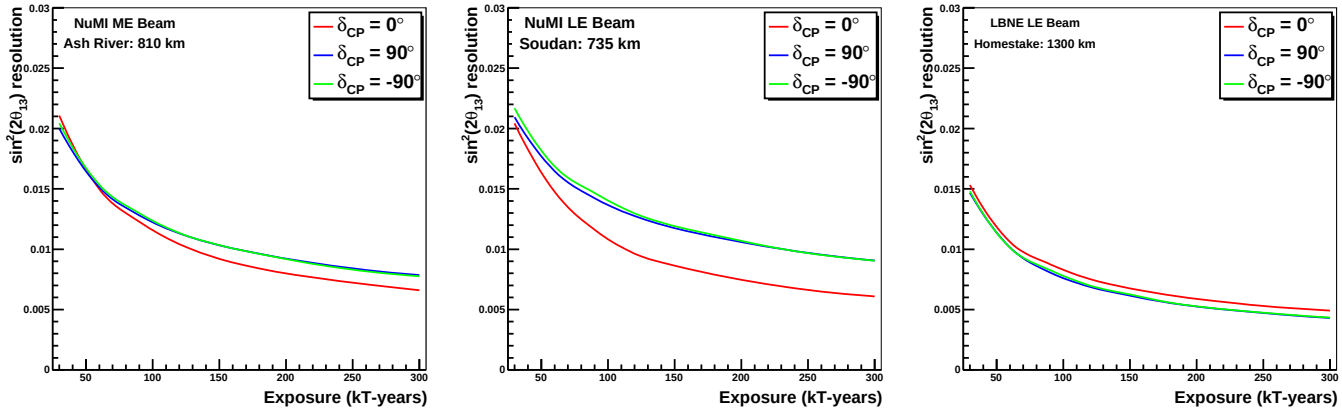

FIG. 12. The 1σ resolution on the measurement of $\sin^2 2\theta_{13} = 0.092$ as a function of exposure in kt.yrs for $\delta_{cp} = 0$ (red), $\pi/2$ (blue), $-\pi/2$ (green). The plots from left to right are for Ash River, Soudan, and Homestake. **The mass hierarchy is assumed to be known.**

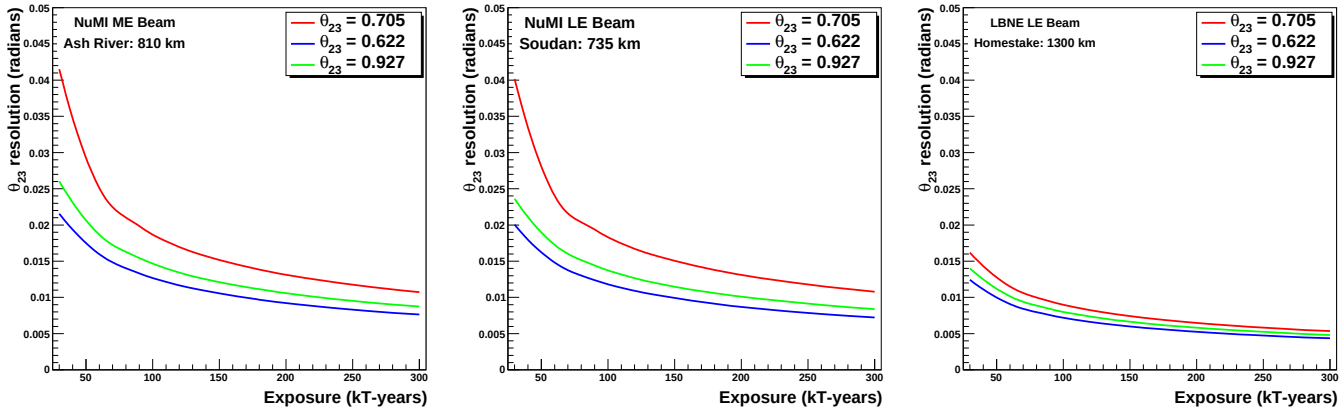

FIG. 13. The 1σ resolution on the measurement of $\sin^2 2\theta_{23}$ from $\nu_\mu \to \nu_\mu$ and $\nu_\mu \to \nu_e$ oscillations as a function of exposure in kt.yrs for different values of $\sin^2 2\theta_{23}$. Neutrino and anti-neutrino running are combined in the ratio of 1:1. The plots from left to right are for Ash River, Soudan, and Homestake. **The mass hierarchy is assumed to be known.**

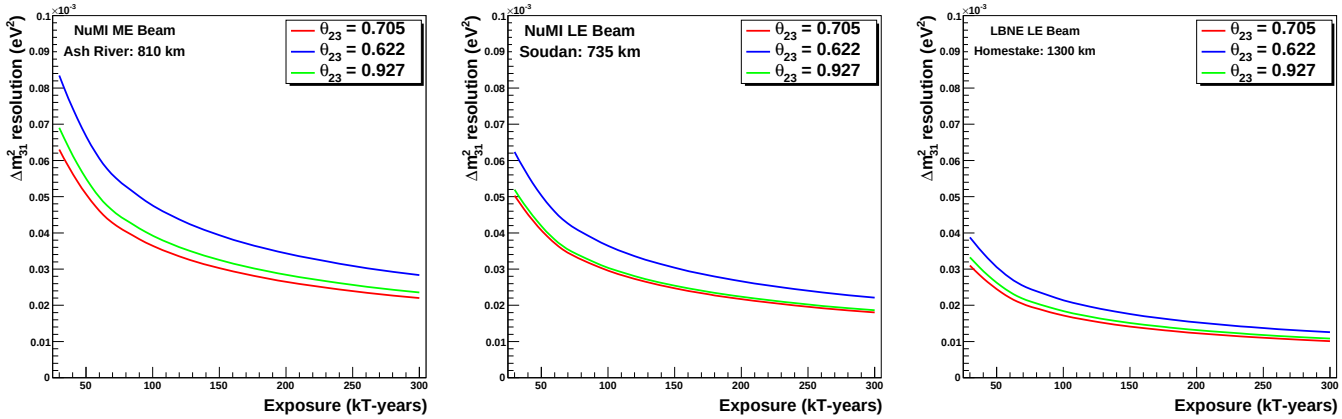

FIG. 14. The 1σ resolution on the measurement of $|\Delta m^2_{31}| = 2.35 \times 10^{-3}$ eV^2 from $\nu_\mu \to \nu_\mu$ and $\nu_\mu \to \nu_e$ oscillations as a function of exposure in kt.yrs for different values of $\sin^2 2\theta_{23}$. Neutrino and anti-neutrino running are combined in the ratio 1:1. The plots from left to right are for Ash River, Soudan, and Homestake. **The mass hierarchy is assumed to be known.**

E. Searches for New Physics

In addition to precision measurements of the standard three-flavor neutrino oscillation parameters, LBNE is also well-suited for new physics searches in the neutrino sector. For example, the experiment is sensitive to non-standard neutrino interactions and active-sterile neutrino mixing, provided that these effects are not too weak.

1. Non-standard Interactions

NC non-standard interactions (NSI) can be understood as non-standard matter effects that are visible only in a far detector at a sufficiently long-baseline. This is where LBNE has a unique advantage compared to other long-baseline experiments (except atmospheric neutrino experiments, which are, however, limited by systematic effects). NC NSI can be parameterized as new contributions to the MSW matrix in the neutrino-propagation Hamiltonian:

$$H = U \begin{pmatrix} 0 & & \\ & \Delta m^2_{21}/2E & \\ & & \Delta m^2_{31}/2E \end{pmatrix} U^\dagger + \tilde{V}_{\rm MSW}\,, \tag{5}$$

with

$$\tilde{V}_{\rm MSW} = \sqrt{2} G_F N_e \begin{pmatrix} 1+\epsilon^m_{ee} & \epsilon^m_{e\mu} & \epsilon^m_{e\tau} \\ \epsilon^{m*}_{e\mu} & \epsilon^m_{\mu\mu} & \epsilon^m_{\mu\tau} \\ \epsilon^{m*}_{e\tau} & \epsilon^{m*}_{\mu\tau} & \epsilon^m_{\tau\tau} \end{pmatrix} \tag{6}$$

Here, U is the leptonic mixing matrix, and the ϵ-parameters give the magnitude of the NSI relative to standard weak interactions. For new physics scales of few $\times$ 100 GeV, we expect $|\epsilon| \lesssim 0.01$.

To assess the sensitivity of LBNE to NC NSI, the NSI discovery reach is defined in the following way: After simulating the expected event spectra, assuming given "true" values for the NSI parameters, one attempts a fit assuming no NSI. If the fit is incompatible with the simulated data at a given confidence level, one would say that the chosen "true" values of the NSI parameters are within the experimental discovery reach. As an example of the reach for new physics, figure 15 shows the NSI discovery reach of a Phase-2 LBNE at Homestake for the case where only one of the $\epsilon^m_{\alpha\beta}$ parameters is non-negligible at a time [27]. It can be concluded from the figure that such an experiment would be able to improve model-independent bounds on NSI in the e–μ sector by a factor of two, and in the e–τ sectors by an order of magnitude.

2. Long-range Interactions

The small scale of neutrino-mass differences implies that minute differences in the interactions of neutrinos and antineutrinos with background sources can be detected through perturbations to the time evolution of the flavor eigenstates. The longer the experimental baseline, the higher the sensitivity to a new long-distance potential acting on neutrinos. For example, some of the models for such long-range interactions (LRI) as described in [31] could contain discrete symmetries that stabilize the proton and a dark matter particle and thus provide new connections between neutrino, proton decay and dark matter experiments. The longer baseline of LBNE coupled with the expected precision of better than 1% on the ν_μ and $\bar{\nu}_\mu$ oscillation parameters improves the sensitivity to LRI beyond that possible by the current generation of long-baseline neutrino experiments.

3. Search for Active-Sterile Neutrino Mixing

Searches for evidence of active sterile neutrino mixing at LBNE can be conducted by examining the NC event rate at the Far Detector and comparing it to a precision measurement of the expected rate from the near detector. Observed deficits in the NC rate could be evidence for active sterile neutrino mixing. The latest such search in a long baseline experiment was conducted by the MINOS experiment [32]. The expected rate of NC interactions with visible energy > 0.5 GeV in LBNE is approximately 5K events over five years (see Table IV). The NC identification efficiency is high with a low rate of ν_μ CC background misidentification as shown in Table V. LBNE will provide a unique opportunity to revisit this search with higher precision over a large range of neutrino energies.

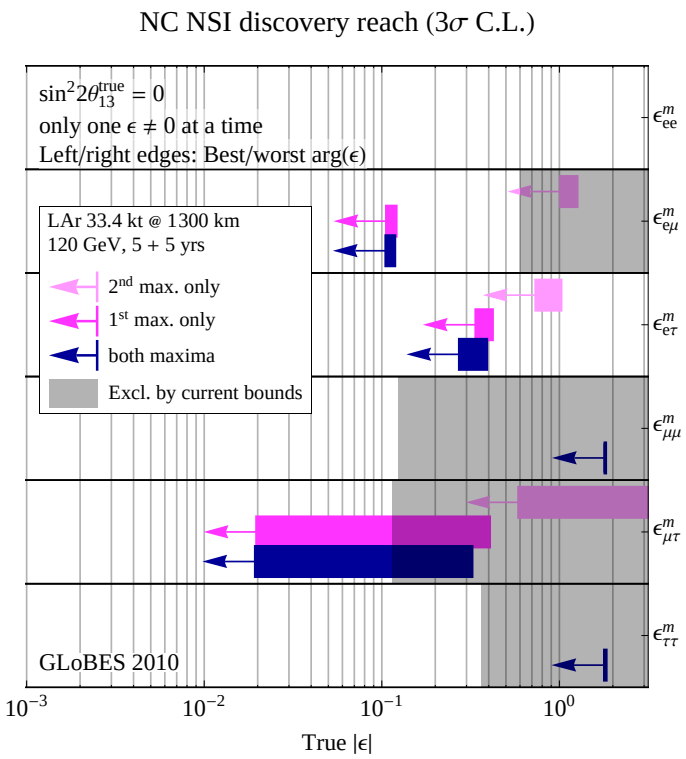

FIG. 15. Non-standard interaction discovery reach in a 34kt LAr-TPC at Homestake. The left and right edges of the error bars correspond to the most favorable and the most unfavorable values for the complex phase of the respective NSI parameters. The gray shaded regions indicate the current model-independent limits on the different parameters at 3 σ [28–30].

F. Summary

The fraction of the possible CP-violating phase angles for which the mass hierarchy can be resolved at 2 or 3 σ is shown in Figure 16 as a function of detector mass. Results are plotted for each detector alone and for a global analysis using the LAr, NOvA, and T2K results. For the Minnesota sites, it is assumed that NOvA would continue to run concurrently with the LAr detector for a total NOvA run of 16 years (NOvA(16)). For the South Dakota site, NOvA would stop data taking when the new beamline turned on, for a total NOvA run of 6 years (NOvA(6)). The fraction of the possible CP-violating phase angles for which CP violation can be resolved at 3 or 5 σ is shown in Figure 17 as a function of detector mass. The opposite mass hierarchy hypothesis is included in the estimation of the significance with which CP violation can be measured. Here again, results are provided for the LAr detector alone and for a LAr-NOvA-T2K global analysis. Figure 18 shows the δ_{cp} resolution achievable at each location with the mass hierarchy assumed to be known.

Table VII summarizes the oscillation measurements achievable with different configurations.

The LBNE Reconfiguration Steering Group has identified three experimental choices for Phase I of the next generation long-baseline neutrino experiment: 1) 10kt LAr detector on the surface at Homestake, 2) a 15kt LAr detector underground at Soudan, and 3) a 30 kt LAr detector on the surface at Ash River. Figure 19 summarizes the physics reach for determining the mass hierarchy and CP violation for the three choices alone and in combination with NOvA and T2K neutrino running for 5×10^{21} protons-on-target. The effect of a change in $\sin^2 2\theta_{13}$ by up to $\pm 2\sigma$ from the current value is shown as colored bands. Figure 20 shows the effect of variations in $\sin^2 2\theta_{23}$. Note that for the mass hierarchy and CP violation measurements, it is just as important to know θ_{23} as it is θ_{13}. Figure 21 shows similar plots but for variations in Δm^2_{31}.

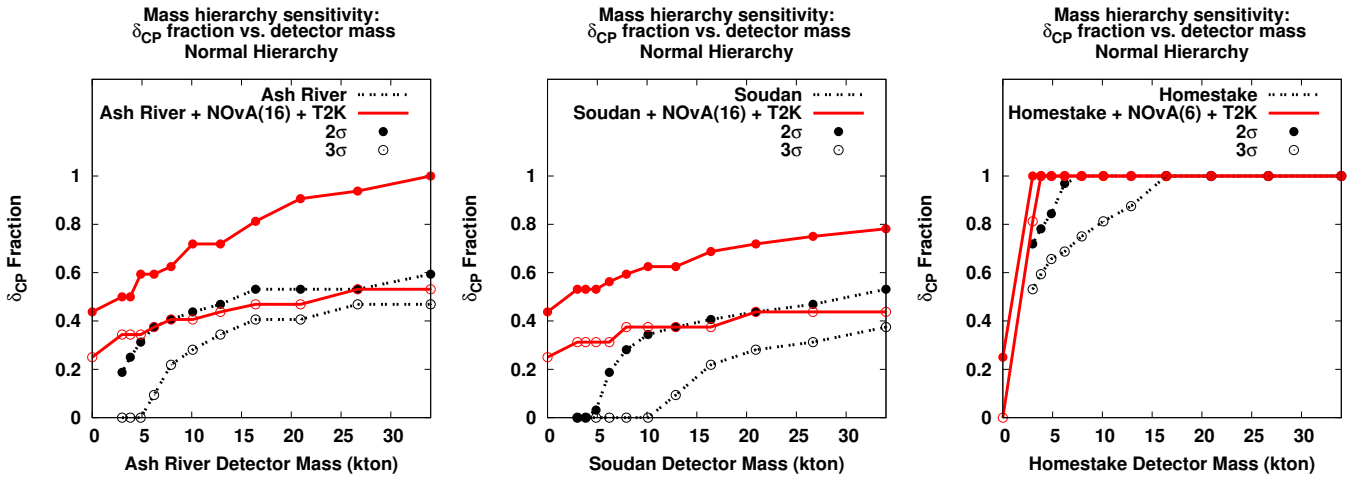

FIG. 16. The fraction of δ_{cp} values for which the mass hierarchy can be resolved at 2/3 σ (solid/open points) as a function of LAr-TPC detector mass. The dashed black line indicates the sensitivty from the experiment alone. The solid red line is the resolution obtained from the combination with T2K (neutrinos only) and NOνA. The plots from left to right are for Ash River, Soudan, and Homestake. The measurements assume $\sin^2 2\theta_{13} = 0.092$, normal hierarchy and a combination of 5yrs of running in neutrino mode with 5 yrs of running in anti-neutrino mode with 700kW. The NuMI LE beam is used with the LAr-TPC at both Soudan and Ash River.

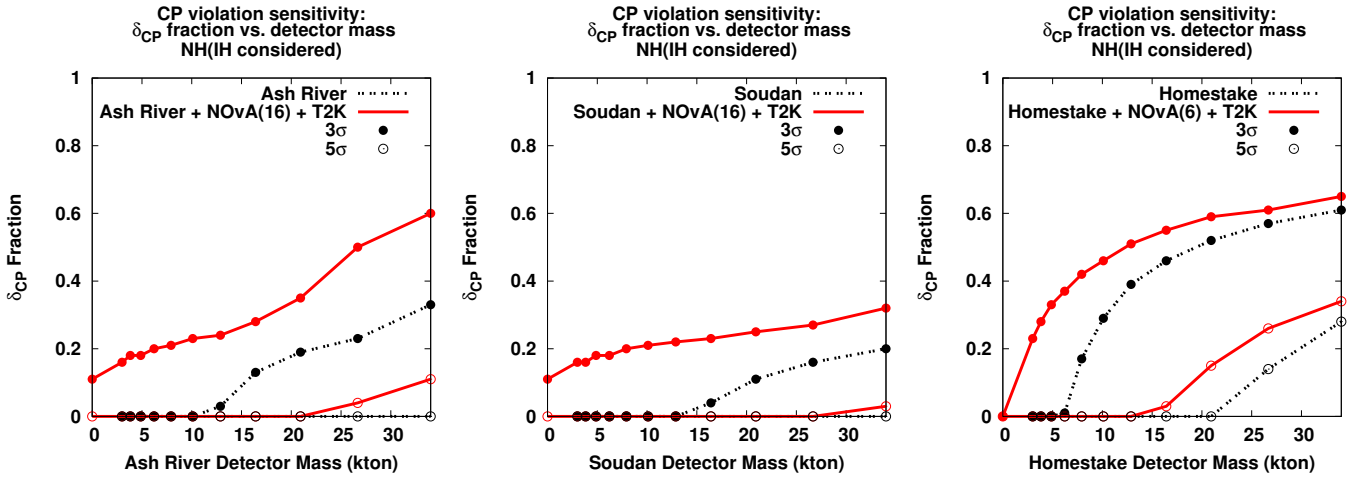

FIG. 17. The fraction of δ_{cp} values for which CP violation can be resolved at 3/5 σ (solid/open points) as a function of LAr-TPC detector mass. The dashed black line indicates the sensitivity from the experiment alone. The solid red line is the resolution obtained from the combination with T2K (neutrinos only) and NOνA. The plots from left to right are for Ash River, Soudan, and Homestake. The measurements assume $\sin^2 2\theta_{13} = 0.092$, normal hierarchy and a combination of 5yrs of running in neutrino mode and 5 yrs of running in anti-neutrino mode with 700kW. The NuMI LE beam is used with the LAr-TPC at both Soudan and Ash River.

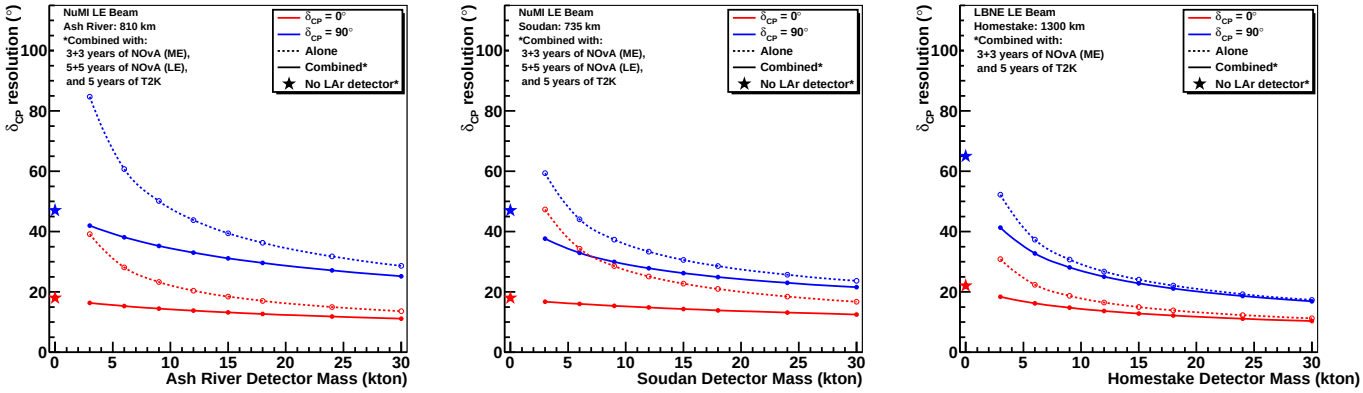

FIG. 18. The 1σ resolution on the measurement of δ_{cp} as a function of LAr-TPC detector mass for $\delta_{cp} = 0$ (red), $\pi/2$ (blue). A tight external constraint on $\theta_{13} = 0.154 \pm 0.005$ is included. The dashed lines are the resolution obtained from each experiment alone. The solid lines include the combination with T2K (neutrino only) and NOνA. The plots from left to right are for Ash River, Soudan, and Homestake. The measurements assume $\sin^2 2\theta_{13} = 0.092$, normal hierarchy and a combination of 5yrs of running in neutrino mode and 5 yrs of running in anti-neutrino mode with 700kW. The NuMI LE beam is used with the LAr-TPC at both Soudan and Ash River. **The mass hierarchy is assumed to be known.** The stars represent the resolutions obtained from the NOνA+T2K combination alone.

TABLE VII. Summary of the oscillation measurements with different configurations given $\theta_{13} = 8.8°, \theta_{23} = 40°, \Delta m^2_{31} = +2.27 \times 10^{-3}\text{eV}^2$. The fraction of δ_{cp} values for which the mass hierarchy (MH) or CP violation (CPV) are determined with 3σ sensitivity are given in the first 2 columns. For the first 2 columns, all correlations and uncertainties on the known mixing parameters, as well as consideration of the opposite mass hierarchy hypothesis, are included. For the estimates of the resolutions on the different oscillation parameters, the mass hierarchy is assumed to be known. The measurements assume 5 years of neutrino running and 5 years of anti-neutrino running at a beam power of 708kW with 6×10^{20} protons-on-target accumulated per year with a LAr-TPC. We assume NOνA will run for a minimum of 3+3 years with the NuMI ME energy beam (NOνA I). An additional 5+5 years of running with NOνA in the NuMI LE beam (NOνA II) is assumed when combining with Soudan and Ash River options. We assume 5×10^{21} protons-on-target total accumulated by T2K ($\sim$ 6 yrs) in neutrino only mode. * These measurements are for the combination of neutrino and anti-neutrino running.

Configuration	MH* fraction of δ (3σ)	CPV* fraction of δ (3σ)	$\sigma(\delta_{cp})$* $0, 90°$	$\sigma(\theta_{13})$* $\delta = 90°$	$\sigma(\theta_{23})$ ν	$\sigma(\theta_{23})$ $\bar{\nu}$	$\sigma(\Delta m^2_{31})$ ν (10^{-3} eV^2)	$\sigma(\Delta m^2_{31})$ $\bar{\nu}$ (10^{-3} eV^2)
Soudan 10kt	0.00	0.00	27,36°	0.70°	1.3°	1.6°	0.045	0.065
Soudan 15kt	0.17	0.05	23,30°	0.60°	1.1°	1.3°	0.036	0.055
Soudan 30kt	0.34	0.18	16,24°	0.45°	0.80°	0.97°	0.028	0.040
Ash River 10kt	0.28	0.00	23,48°	0.60°	1.3°	1.8°	0.058	0.080
Ash River 15kt	0.37	0.10	19,40°	0.50°	1.0°	1.5°	0.048	0.069
Ash River 30kt	0.47	0.27	18,29°	0.40°	0.74°	1.1°	0.035	0.050
Homestake 5kt	0.66	0.00	25,41°	0.60°	0.92°	1.4°	0.035	0.055
Homestake 10kt	0.81	0.27	17,30°	0.40°	0.69°	0.97°	0.025	0.040
Homestake 15kt	0.95	0.43	15,25°	0.30°	0.52°	0.80°	0.020	0.030
Homestake 20kt	1.0	0.50	13,21°	0.25°	0.46°	0.63°	0.018	0.026
NOνA I (6yrs) +T2K (6yrs)	0.0	0.0	22,65°	0.62°				
NOνA I+II (16yrs)+T2K (6yrs)	0.25	0.11	18,47°	0.53°				
Soudan 10kt +NOνA (I+II)+T2K	0.38	0.21	16,30°					
Soudan 15kt +NOνA (I+II)+T2K	0.38	0.23	14,26°					
Soudan 30kt +NOνA (I+II)+T2K	0.45	0.29	12,21°					
Ash River 10kt +NOνA (I+II)+T2K	0.40	0.23	14,34°					
Ash River 15kt +NOνA (I+II)+T2K	0.45	0.25	13,30°					
Ash River 30kt +NOνA (I+II)+T2K	0.50	0.55	13,25°					
Homestake 5kt +NOνA I+T2K	1.00	0.33	15,31°					
Homestake 10kt +NOνA I+T2K	1.00	0.45	12,25°					
Homestake 15kt +NOνA I+T2K	1.00	0.53	12,24°					

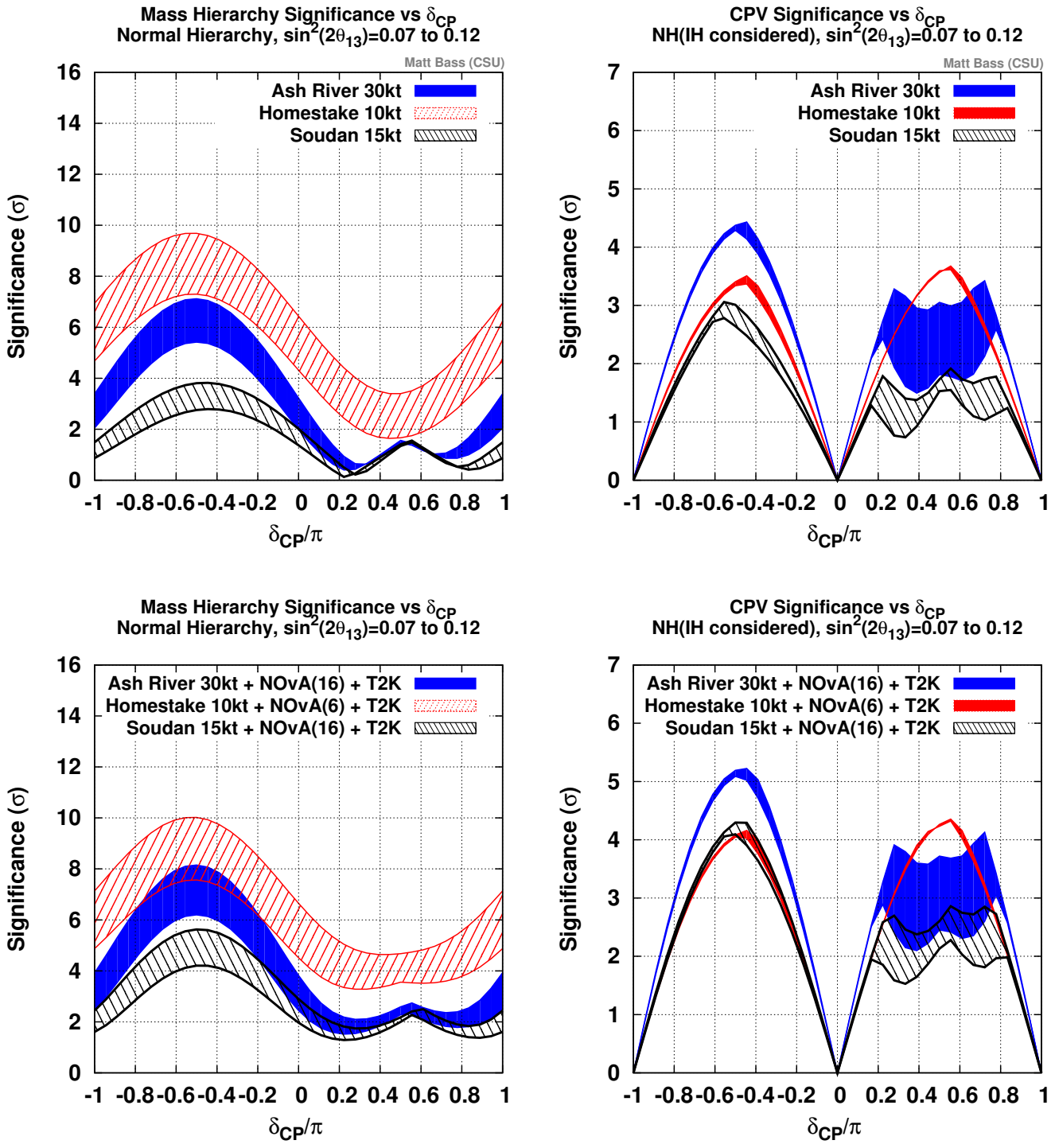

FIG. 19. Comparison between the 3 selected configurations. Significance with which the mass hierarchy is resolved is on the left. The significance with which δ_{cp} is determined to be $\neq 0, \pi$ is on the right. The top set of plots is for the 3 choices alone : 10kt at Homestake, 15kt at Soudan and 30kt at Ash River. The bottom set of plots is for the 3 choices combined with NOνA and T2K running. NOνA is assumed to run for 6 years in combination with LBNE-Homestake and for 16 years in combination with the Minnesota sites. T2K is assumed to run for an integrated 5×10^{21} protons-on-target. The colored bands indicate the change in significance when the central value of $sin^2 2\theta_{13}$ assumed is changed from 0.07 to 0.12.

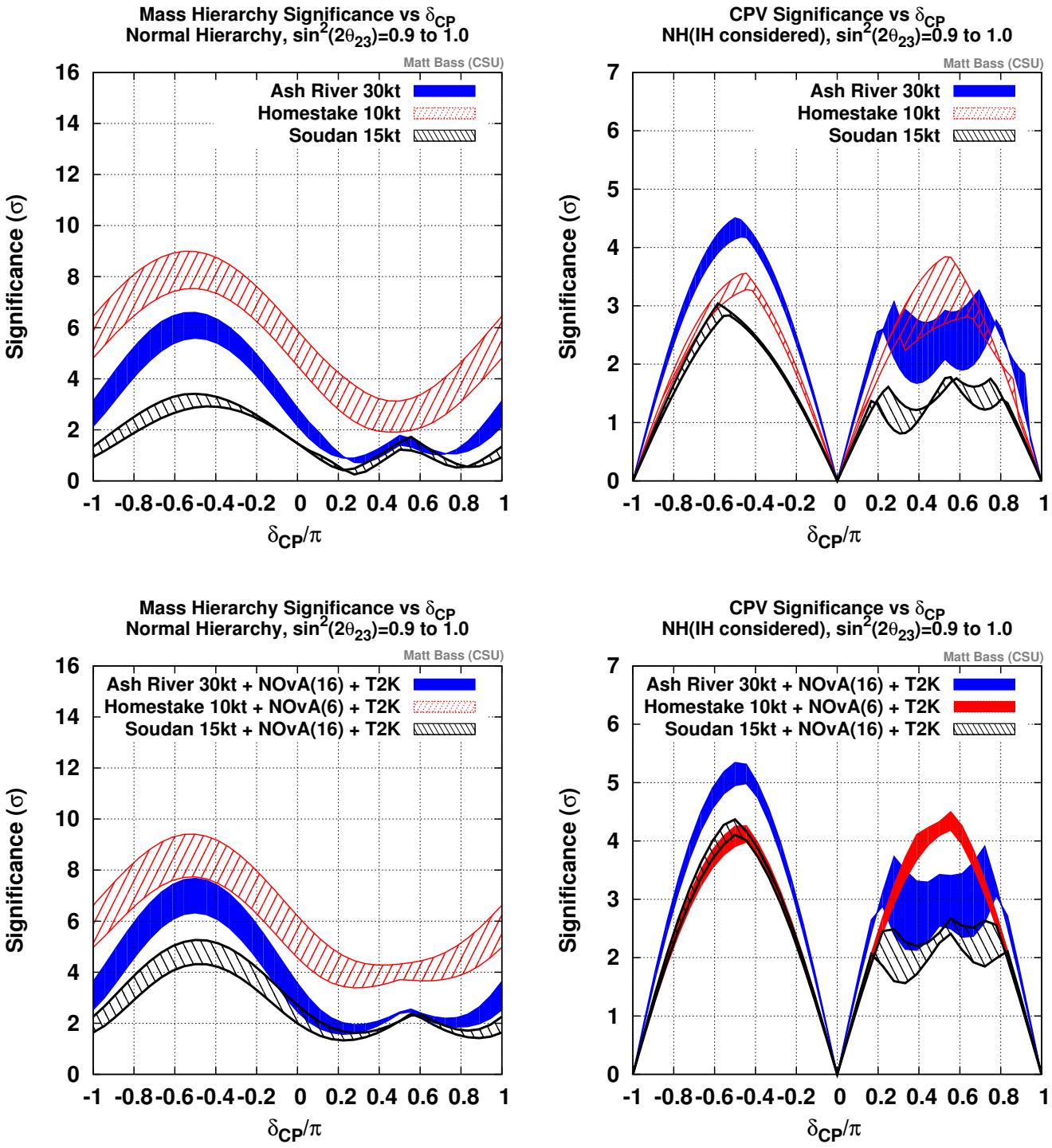

FIG. 20. Same as Figure 19 except showing the effect of varying $\sin^2 2\theta_{23}$ from 0.9 to 1.0.

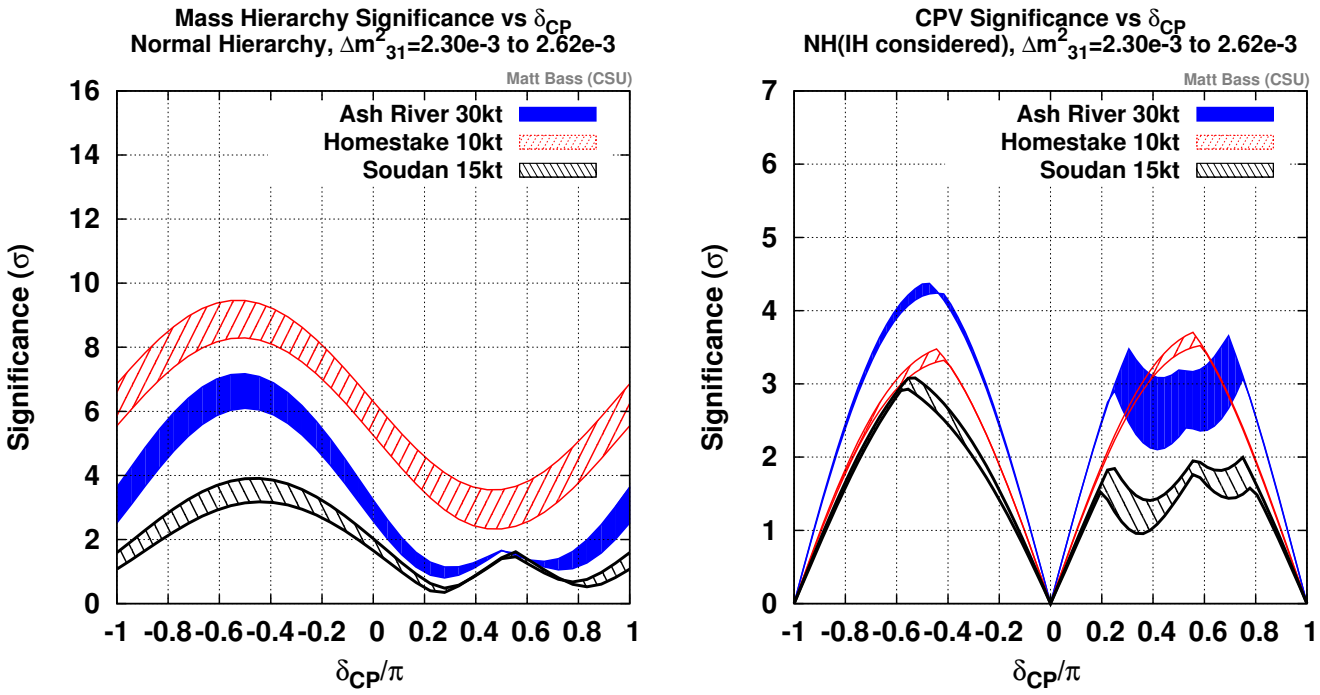

FIG. 21. Same as Figure 19 except showing the effect of varying Δm^2_{31} by $\pm 7\%$.

G. What is the Optimal Baseline for LBNE?

A number of studies have been done to determine the optimal baseline for a next-generation long-baseline neutrino experiment aiming to determine the mass hierarchy and CP violation [33] – most were performed before the value of θ_{13} was known. One might now ask whether or not the distance from Fermilab to Homestake remains an optimal choice for LBNE given the now known value of θ_{13}. To determine the optimal baseline for LBNE with a new neutrino beamline, the LBNE LE beam design described in Table III was modified to produce a beam flux that covered the entire region of the 1st oscillation node at each baseline. The double-parabolic NuMI focusing system was used, since it is highly tunable. The target to horn 1 distance, decay pipe length and off-axis angle were varied to match the baseline. Table VIII summarizes the beam parameters used for each baseline and the estimated signal and background event rates obtained at a 35kt LAr-TPC far detector.

TABLE VIII. The modified LBNE beam configuration used at each baseline to determine the optimal baseline for the next generation long-baseline experiment. The beam parameters were chosen to cover the entirety of the 1st oscillation node at each baseline. The signal and background event rates are for a 35kt LAr-TPC 5+5 years at 700kW (6×10^{20} protons-on-target/year) for $\sin^2(2\theta_{13}) = 0.09,\ \delta_{cp} = 0$, normal hierarchy.

Baseline (km)	Target-Horn 1 distance	Decay pipe length	Off-axis angle	ν_e+$\bar{\nu}_e$ appearance signal	background
300	30cm	280m	2°	480+170	740+450
500	30cm	280m	1.5°	450+150	425+240
750	30cm	280m	1.0°	520+170	350+200
1000	0cm	280m	0°	820+290	434+270
1300	30cm	280m	0°	770+230	310+180
1700	30cm	280m	0°	550+130	170+100
2000	70cm	580m	0°	780+160	321+122
2500	70cm	580m	0°	610+100	140+75
3000	100cm	580m	0°	560+72	100+50

The event spectra expected from in a 35kt LAr-TPC running for 5 years in a 700kW beam at each baseline using the beam configurations described in Table III are shown in Figures 22 (neutrinos) and 23 (anti-neutrinos).

Figure 24 shows the mass hierarchy and CP violation reach for a 35 kton LAr-TPC detector in 10 years of running for various baseline considerations when a different flux was chosen to more appropriately match the baseline. Figure 25 shows the fraction of δ_{cp} values for which CP violation and the mass hierarchy can be determined at the 3σ level or greater as a function of baseline. For determining the CP violation uncertainty, the mass hierarchy is assumed to be unknown and is allowed to change. The optimal baseline for the CP violation measurement is found to be in the range 1000-1500km. A 1300 km distance achieves a $> 5\sigma$ determination of the mass hierarchy for all values of δ_{CP} with a 35 kt detector and simultaneously maintains the highest sensitivity for CP violation. Hence, the distance from Fermilab to Homestake remains an optimal baseline given what is now known about the value of θ_{13}.

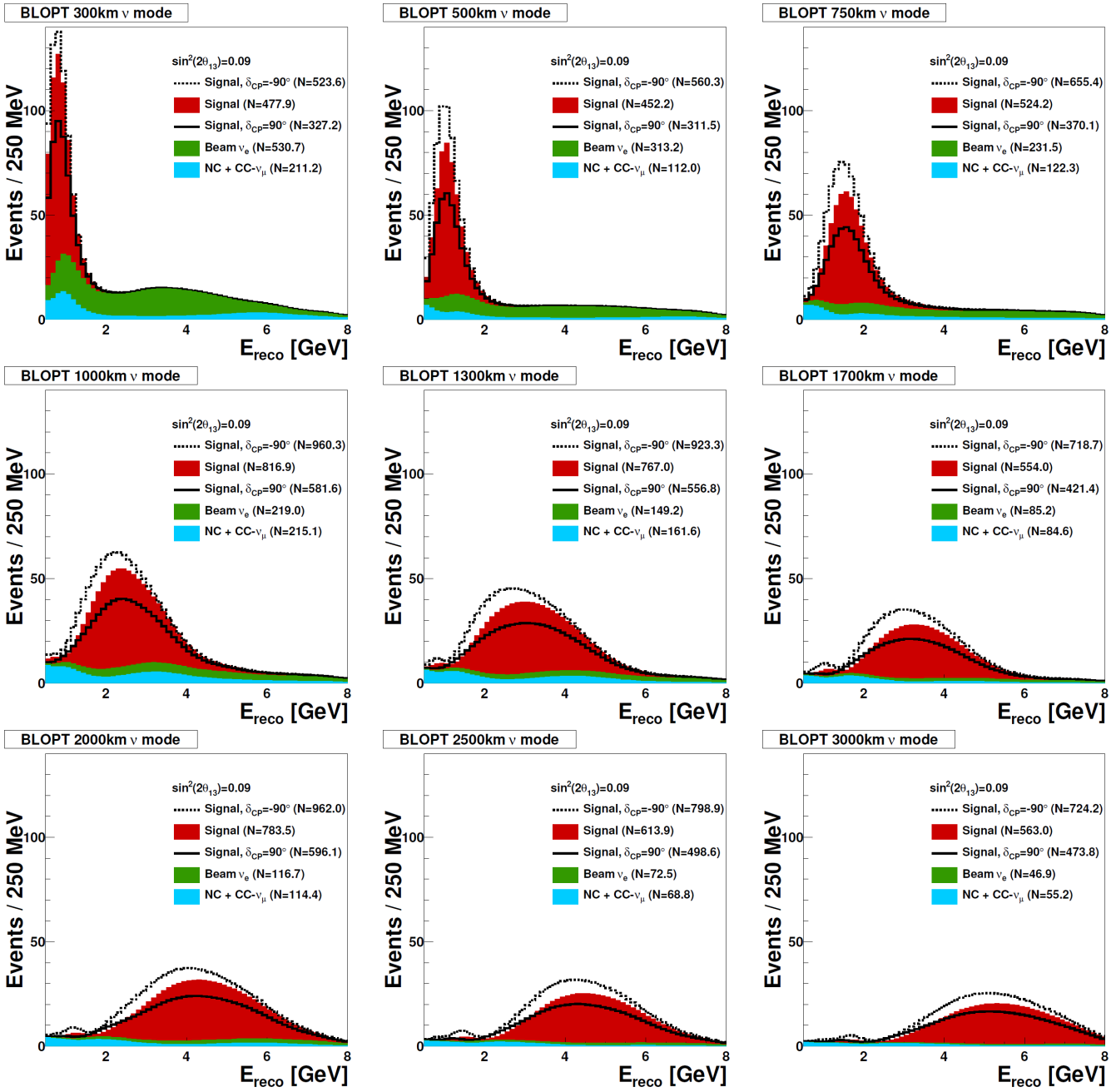

FIG. 22. Neutrino event spectra in a 35 kt LAr-TPC at different baselines with optimized LBNE beam tunes. Projections assume $\sin^2 2\theta_{13} = 0.09$ and a running time of 5 years with a 700kW beam.

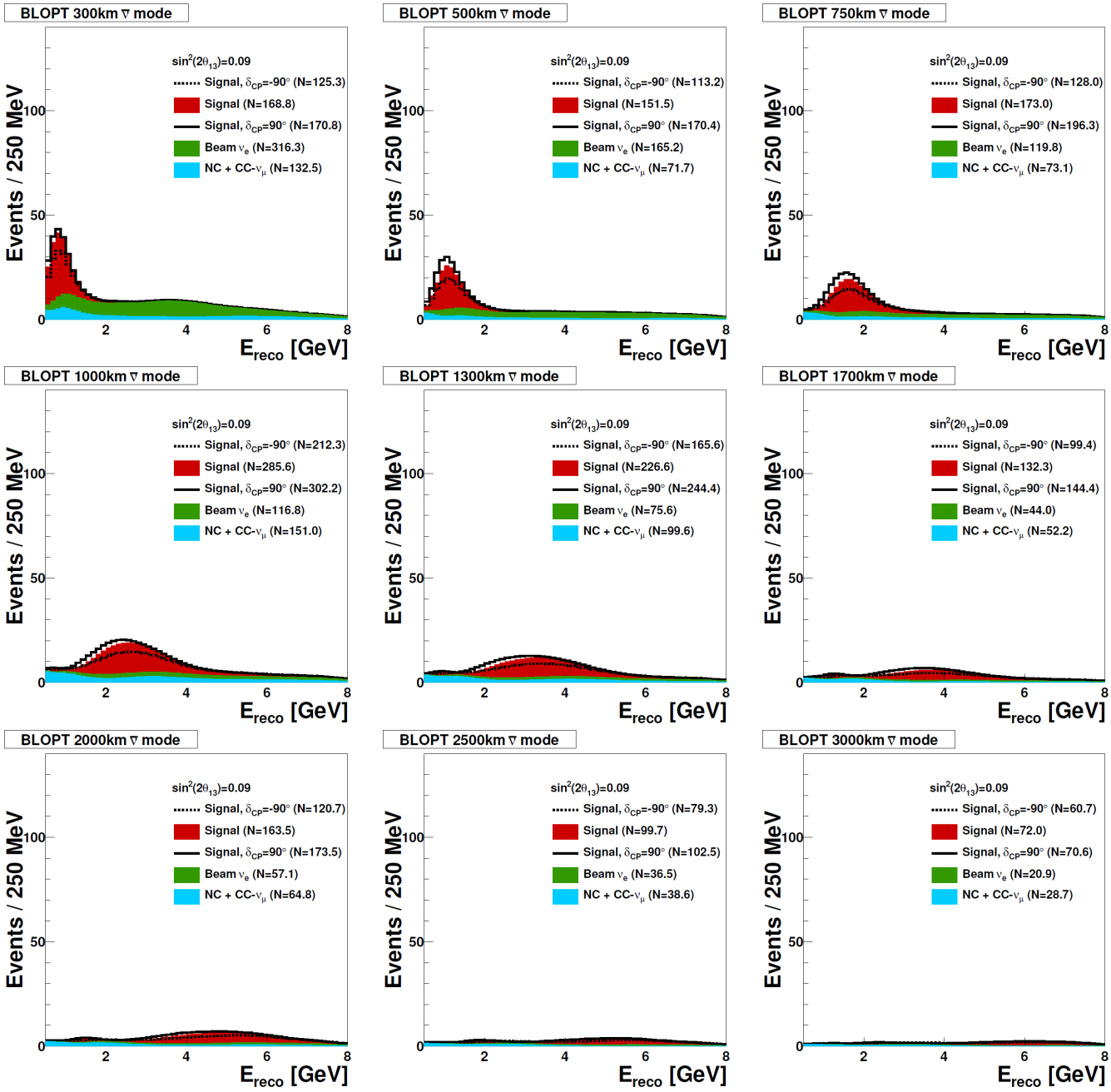

FIG. 23. Anti-neutrino event spectra in a 35 kt LAr-TPC at different baselines with optimized LBNE beam tunes. Projections assume $\sin^2 2\theta_{13} = 0.09$ and a running time of 5 years with a 700kW beam.

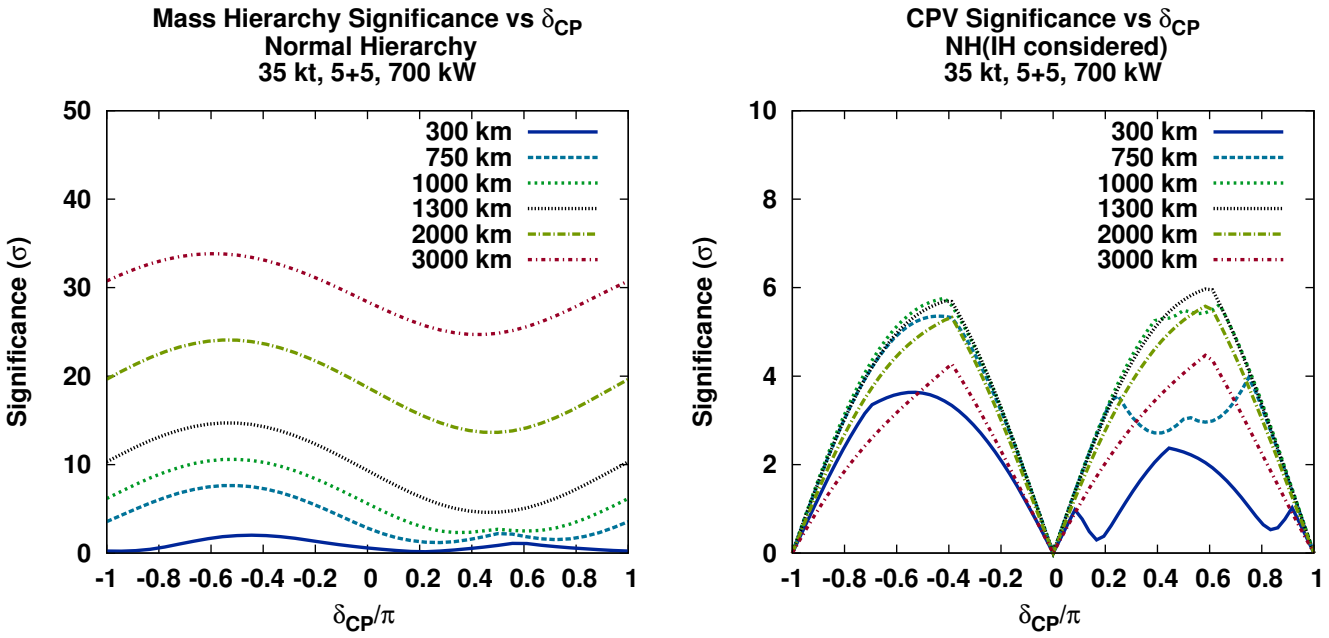

FIG. 24. Significance with which the mass hierarchy (left) and CP violation (right) can be determined as a function of δ_{CP} for a 35 kt LAr detector in 5+5 years of neutrino + anti-neutrino running for various baselines ranging from 300 km up to 3000 km. In each case, the beam was adjusted to more appropriately match the baseline. Projections assume $\sin^2 2\theta_{13} = 0.09$.

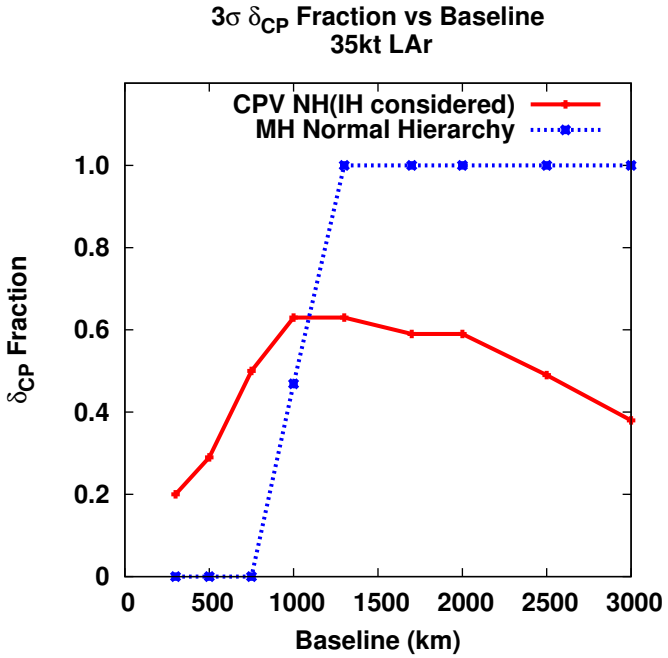

FIG. 25. The fraction of δ_{cp} values for which CP violation and the mass hierarchy can be determined at the 3σ level or greater as a function of baseline. The LBNE beam design was optimized for each base-line. Projections assume $\sin^2 2\theta_{13} = 0.09$.

IV. NON-ACCELERATOR PHYSICS REACH

A large liquid argon TPC, when sited underground, has significant capabilities for addressing diverse physics topics, including proton decay, and atmospheric and supernova neutrinos. These capabilities are described in detail in reference [25]. For non-beam physics, no external trigger will be available, and therefore the key issue is selection of signal from background, assuming suitable triggering can be implemented. Photon collection will likely be required. Since backgrounds are dominated by cosmic rays, physics reach for a given detector size depends primarily on depth. Table IX summarizes expected signal rates. Proton decay and atmospheric neutrino events are, like beam events, ∼GeV scale, and should in principle be quite cleanly identifiable in a LArTPC: see Figs. 26 and 27. Proton decay events, although distinctive, would be extremely rare, and hence highly intolerant of background; in contrast, atmospheric neutrinos (which are background for proton decay) have a higher rate and could tolerate some background. The signatures of individual supernova burst neutrino interaction events are much less clean. With only a few tens of MeV of energy, these neutrinos will create small tracks involving only a few adjacent wires: see Fig. 28. For diffuse "relic" supernova events which arrive singly, the very low expected signal rate makes their selection overwhelmingly difficult, and we will not consider them further here. A nearby core collapse is more promising: it will provide a pulse of low energy events all arriving within ∼30 seconds, so that we can hope to make a meaningful measurement of signal over a (well-known) background.

TABLE IX.

Physics	Energy range	Expected signal rate (events kton^{-1}s^{-1})
Proton decay	$\sim$ GeV	$< 2 \times 10^{-9}$
Atmospheric neutrinos	$0.1 - 10$ GeV	$\sim 10^{-5}$
Supernova burst neutrinos	few-50 MeV	$\sim$ 3 in 30 s at 10 kpc
Diffuse supernova neutrinos	20-50 MeV	$< 2 \times 10^{-9}$

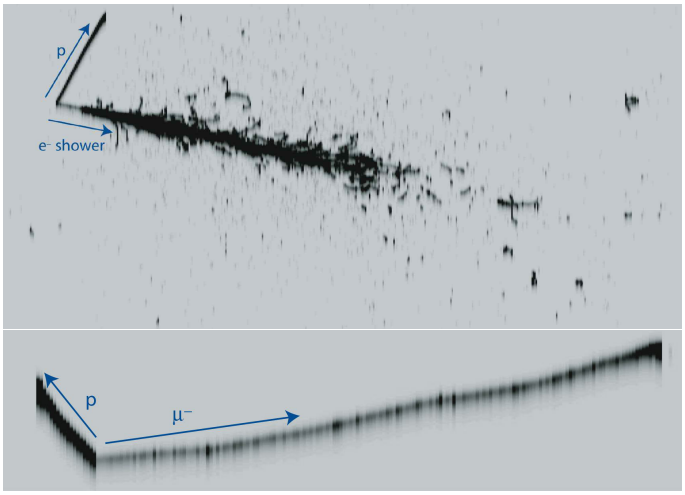

FIG. 26. Example ν_e and ν_μ CC atmospheric neutrino events in liquid argon from reference [35].

We will consider the physics reach as a function of detector mass and depth for proton decay, supernova bursts and atmospheric neutrinos. (Solar neutrinos will not be considered; with mostly <10 MeV energies, they require stringent control of background. Other than providing a ν_e calibration in argon for supernova neutrinos, they are not likely to tell us anything not already known in the detectors under consideration.)

A. Searches for baryon number non-conservation

Searches for baryon-number-violating processes are highly motivated by grand unified theories. Even a single event could be evidence of physics beyond the Standard Model. Current limits are dominated by Super-K [34]; however for

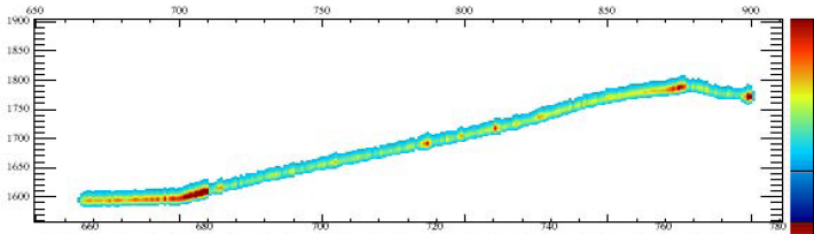

FIG. 27. LArSoft simulation of $p \to K^+\bar{\nu}$ decay with $K^+ \to \mu^+ \to e^+$ in the MicroBooNE geometry. The drift time is along the vertical axis. The wire number is along the horizontal axis (3-mm wire spacing).

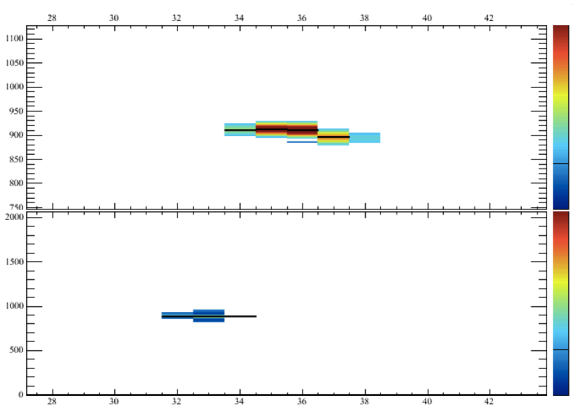

FIG. 28. LArSoft simulation of a 10 MeV electron (which would resemble a supernova neutrino event) in the MicroBooNE geometry (3-mm wire spacing). There are four reconstructed hits (black bands) on five adjacent wires. This event would create signals on about four wires with 5-mm spacing. The drift time is on the vertical axis, and the wire number is on the horizontal axis.

some predicted modes, most prominently $p \to K^+\bar{\nu}$, efficiency for water Cherenkov detectors is low, and detectors which can cleanly reconstruct kaon decay products have a substantial efficiency advantage. Other modes for which LArTPCs have an edge include $n \to e^-K^+$ and $p \to e^+\gamma$. Figure 29 shows the expected limit as a function of time for $p \to K^+\bar{\nu}$. According to this plot, approximately 10 kton of LAr is required to improve the limits significantly beyond continued Super-K running.

In LAr, the most pernicious background for proton decay with kaon final states comes from cosmic rays that produce entering kaons in photonuclear interactions in the rock near the detector. Backgrounds as a function of depth have been studied for LAr in references [35, 36]. These studies show that proton decay searches can be successful at moderate depth via reduction of fiducial mass or in conjunction with a high-quality veto, but cannot be done at the surface. Among the sites under consideration, Homestake would be excellent. Soudan would likely be acceptable, although it would require some reduction in fiducial mass. Proton decay searches are not feasible for any of the surface options.

B. Atmospheric Neutrinos

Atmospheric neutrinos are unique among sources used to study oscillations: the oscillated flux contains neutrinos and antineutrinos of all flavors, and matter effects play a significant role. The expected interaction rate is about 285 events per kton-year. The excellent CC/NC separation and the ability to fully reconstruct the hadronic final state in CC interactions in an LArTPC would enable the atmospheric neutrino 4-momentum to be fully reconstructed. This would enable a higher-resolution measurement of L/E to be extracted from atmospheric-neutrino events in an LArTPC compared to the measurements obtained from Super-K, and would provide good sensitivity to mass hierarchy and to the octant of θ_{23}. Since the oscillation phenomenology plays out over several decades in energy and path length,

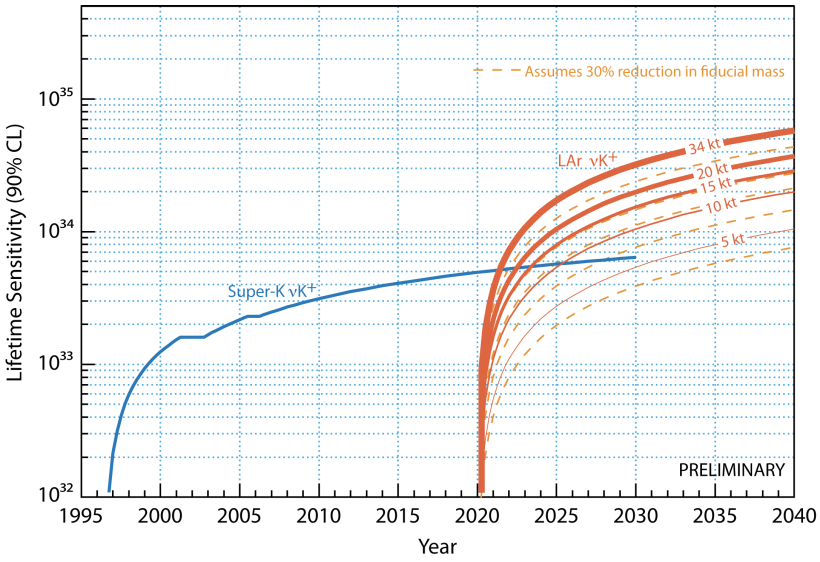

FIG. 29. Proton decay lifetime limit for $p \to K^+\bar{\nu}$ as a function of time for Super-Kamiokande compared to different LAr masses at the 4850 level starting in 2020. The dashed lines show the effect of a 30% reduction of fiducial mass, conservatively assumed for a Soudan-depth detector. The limits are at 90% C.L., calculated for a Poisson process including background assuming that the detected events equal the expected background. (Figure from J. Raaf.)

atmospheric neutrinos are very sensitive to alternative explanations or subdominant new physics effects that predict something other than the characteristic L/E dependence predicted by oscillations in the presence of matter.

Because atmospheric neutrinos are somewhat more tolerant of background than proton decay, a depth which is sufficient for a proton decay search should also be suitable for atmospheric neutrinos. For 4850 ft depth, a veto should not be necessary, and one can assume full fiducial mass; at Soudan depth, a 1 meter fiducial cut should be adequate. Figure 30 shows expected sensitivity to mass hierarchy: for ten years of running, a Soudan-depth 20 kton detector could rival beam sensitivity, and even a 10 kton detector would add to world knowledge.

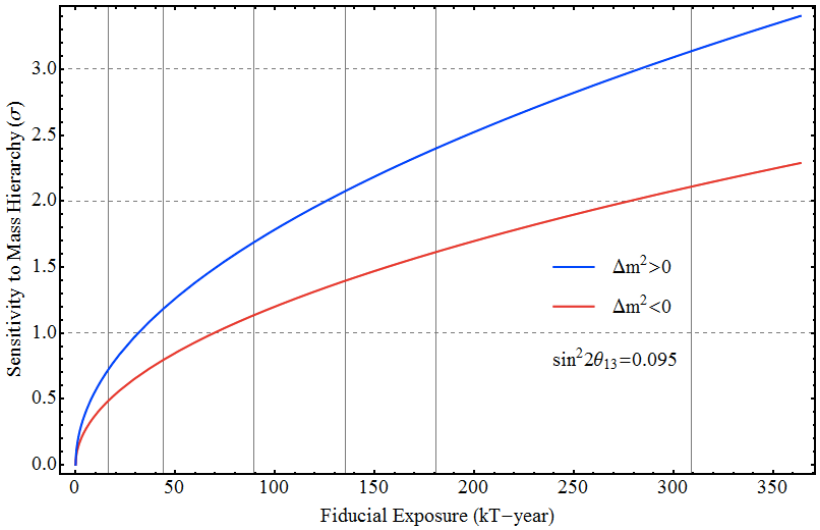

FIG. 30. Sensitivity to mass hierarchy using atmospheric neutrinos as a function of fiducial exposure in a LAr detector. (Figure from H. Gallagher, J. Coelho, A. Blake.)

C. Core Collapse Supernova Neutrinos

A nearby core-collapse supernova will provide a wealth of information via its neutrino signal (see [37, 38] for reviews). The neutrinos are emitted in a burst of a few tens of seconds duration. Energies are in the few tens of MeV range, and luminosity is divided roughly equally between flavors. Ability to measure and tag the different flavor components of the spectrum is essential for extraction of physics and astrophysics from the signal. Currently, world-wide sensitivity is primarily to electron anti-neutrinos, via inverse beta decay on free protons, which dominates the interaction rate in water and liquid scintillator detectors. Liquid argon has a unique sensitivity to the *electron neutrino* component of the flux, via the absorption interaction on ^{40}Ar, $\nu_e + {}^{40}\mathrm{Ar} \rightarrow e^- + {}^{40}\mathrm{K}^*$. In principle, this interaction can be tagged via the de-excitation gamma cascade. About 3000 events would be expected in 34 kton of liquid argon for a supernova at 10 kpc; the number of signal events scales with mass and the inverse square of distance as shown in Fig. 31. For a collapse in the Andromeda galaxy, a 34-kton detector would expect about one event. This sensitivity would be lost for a smaller detector. However even a 5 kton detector would gather a unique ν_e signal from within the Milky Way.

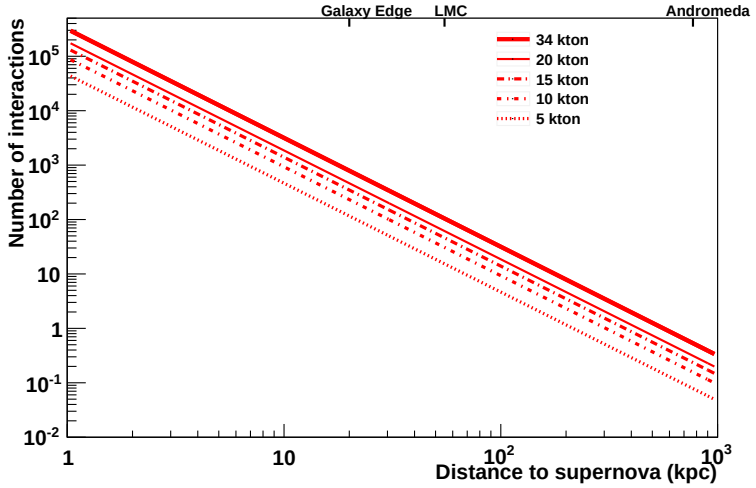

FIG. 31. Number of supernova neutrino interactions in a LAr detector as a function of distance to the supernova, for different detector masses. Core collapses are expected to occur a few times per century, at a most-likely distance of about 10-15 kpc.

As noted above, due to their low energy, supernova events are subject to background, although the short-timescale burst nature of the signal means that the background can be well known and subtracted. Muons and their associated Michel electrons can in principle be removed. Radioactive decays, including cosmogenic spallation products, tend to make <10 MeV signals. They lie below the main supernova signal range, but inhabit a potential region of interest for physics signatures. Preliminary studies from reference [39], extended for cosmic ray rates on the surface, suggest that while Soudan depth is likely acceptable, the surface cosmic-ray associated signal rates are daunting. It will require at least a few orders of magnitude of background rejection to pull the signal from background. While more work needs to be done to determine the extent to which the background can be mitigated, a surface option is highly unfavorable for supernova neutrino physics.

D. Summary

Although more work needs to be done to understand backgrounds at shallow depth, the following findings are fairly robust:

- Proton decay capabilities as a function of depth are the best documented, and a search at the surface seems impossible. A modest fiducial mass reduction would be required at Soudan. A detector mass of at least 10 kton would be needed for competitiveness.
- For atmospheric neutrinos, less is known about signal selection on the surface; however it is probably extremely difficult. Soudan depth is acceptable. Underground, a 20 kton detector would be needed for competitiveness, although a smaller detector could still provide useful information.

- For supernova burst neutrinos, selection of signal events over background at the surface will be a daunting task, and information will be highly degraded even in the best case. Soudan depth would be acceptable. More mass is better, but even a 5-kton detector would provide a unique ν_e-flavor supernova signal.

The overall conclusions are: a reasonably-sized detector sited at 4850 ft depth would provide excellent opportunities for a diverse range of physics topics. Soudan depth requires only modest compromise in physics reach. At the surface, capabilities for non-beam physics are extremely poor.

V. SUMMARY

The results presented here show that the CP-violating phase δ and the neutrino hierarchy can be determined with a number of the options being considered. The accessible range of δ and the confidence in the hierarchy determination increases with detector mass. For shorter baselines, results from the T2K experiment in Japan are required to establish the hierarchy.

The options with a longer baseline and wide-band beam can observe multiple oscillation peaks and the valleys between them. This provides broader sensitivity to neutrino oscillation physics beyond that described by the 3×3 PMNS matrix.

The search for proton decay and the study of atmospheric neutrinos and neutrinos from nearby supernova explosions can be successfully carried out by a liquid argon detector underground, but not one on the surface.

[1] R.N. Mohapatra *et. al.* "'The Theory of Neutrinos: A White Paper".Rept.Prog.Phys. **70** (2007) 1757. arXiv:hep-ph/0510213v2.

[2] F.P. An *et. al.* [Daya Bay Collaboration] "Observation of electron-antineutrino disappearance at Daya Bay". Phys.Rev.Lett. **108** (2012) 171803. arXiv:hep-ex/1203.1669.

[3] J.K. Ahn *et. al.* [RENO Collaboration] "Observation of Reactor Electron Antineutrino Disappearance in the RENO Experiment." arXiv:1204.0626 [hep-ex], 2012.

[4] G.L. Fogli *et. al.* "Evidence of $\theta_{13} > 0$ from global neutrino data analysis". Phys.Rev. D84 (2011) 053007. arXiv:1106.6028 [hep-ph]

[5] K. Nakamura et al. (Particle Data Group), "The Review of Particle Physics". J. Phys. G 37, 075021 (2010).

[6] M. Freund, M. Lindner, S.T. Petcov and A. Romanino, "Testing matter effects in very long baseline neutrino oscillation experiments".Nucl. Phys. B 578 (2000) 27.

[7] J.A. Formaggio and G.P. Zeller, "From eV to EeV: Neutrino Cross Sections Across Energy Scales", to be published in Rev. Mod. Phys. (2012)

[8] D. Casper, Nucl. Phys. Proc. Suppl. **112**, 161 (2002), hep-ph/0208030.

[9] E. Hawker, proceedings of the 2nd International Workshop on Neutrino-Nucleus Interactions in the Few-GeV Region, Irvine, CA, 2002, unpublished, `http://www.ps.uci.edu/ nuint/proceedings/hawker.pdf`

[10] "LBNE Liquid Argon TPC Detector Case Study" LBNE-doc-3600

[11] The LArSoft Collaboration, `https://plone4.fnal.gov:4430/P1/Main/wiki/LArSoft/LArSoft`

[12] A. Ankowski *et al.* [ICARUS Collaboration], Acta Physica Polonica B **41**, 103 (2010).

[13] S. Amoruso *et al.* [ICARUS Collaboration], Eur. Phys. J. **C33**, 233 (2004).

[14] A. Ankowski *et al.* [ICARUS Collaboration], Eur. Phys. J. **C48**, 667 (2006).

[15] "A Large Liquid Argon Time Projection Chamber for Long-baseline Off-Axis Neutrino Oscillation Physics with the NuMI Beam", Submitted to the NuSAG committee, 2006, FERMILAB-FN-0776-E.

[16] "A Proposal for a Detector 2 km Away from the T2K Neutrino Source", `http://www.phy.duke.edu/~cwalter/nusag-members/`.

[17] P. Huber, M. Lindner, W. Winter, "Simulation of long-baseline neutrino oscillation experiments with GLoBES". Comput. Phys. Commun. **167** (2005) 195. arXiv:hep-ph/0407333v1.

[18] P. Huber, M. Lindner, T. Schwetz, and W. Winter, "First hint for CP violation in neutrino oscillations from upcoming superbeam and reactor experiments", arXiv:0907.1896.

[19] I. Ambats *et. al.*, NOvA Collaboration, "NOvA proposal to build a 30-kiloton off-axis detector to study neutrino oscillations in the Fermilab NuMI beamline",hep-ex/0503053.

[20] M. Fechner, "Détermination des performances attendues sur la recherche de l'oscillation $\nu_\mu \to \nu_e$ dans l'experiénce T2K depuis l'étude des données recueilles dans l'éxperience K2K", Ph.D thesis, Université Paris VI, 2006.

[21] Kato, Proceedings of Neutrino 2008, 2008.

[22] J. E. Campagne, M. Maltoni, M. Mezzetto, M. and T. Schwetz, "Physics potential of the CERN-MEMPHYS neutrino oscillation project", JHEP **04** 003 (2007), hep-ph/0603172.

[23] V.A. Kudryatsev *et. al.*, "Muon-induced background for beam neutrinos at the surface". Available at `http://www.fnal.gov/directorate/lbne_reconfiguration/index.shtml`.

[24] M. Bishai *et. al.*, "The Science and Strategy for a Long-Baseline Neutrino Experiment Near Detector". Available at `http://www.fnal.gov/directorate/lbne_reconfiguration/index.shtml`.

[25] T. Akiri *et al.* [LBNE Collaboration] "The 2010 Interim Report of the Long-Baseline Neutrino Experiment Collaboration Physics Working Groups" arXiv:1110.6249

[26] P. Adamson *et al.* [MINOS Collaboration] "Search for the disappearance of muon antineutrinos in the NuMI neutrino beam." FERMILAB-PUB-11-357-PPD, BNL-96122-2011-JA, Phys.Rev.D84:071103,2011. arXiv:1108.1509

[27] arXiv:1010.3706 and private communication with Joachim Kopp.

[28] S. Davidson, C. Pena-Garay, N. Rius, and A. Santamaria, hep-ph/0302093.

[29] M.C. Gonzalez-Garcia, and M. Maltoni, Phys. Rept. **460**, 1 (2008), arXiv:0704.1800 [hep-ph].

[30]

[31] H. Davoudiasl, H.S. Lee and W. J. Marciano, Phys. Rev. D 84 031009 (2011) arXiv:1102.5352[hep.ph]

[32] P. Adamson *et al.* [MINOS Collaboration] Phys.Rev.D81:052004,2010

[33] V. Barger, P. Huber, D. Marfatia, W. Winter, Phys. Rev. D76 053005 (2007)

[34] H. Nishino *et al.* [Super-Kamiokande Collaboration], Phys. Rev. Lett. **102**, 141801 (2009) [arXiv:0903.0676 [hep-ex]].

[35] A. Bueno *et al.*, JHEP **0704**, 041 (2007) [arXiv:hep-ph/0701101].

[36] A. Bernstein, M. Bishai, E. Blucher, D. B. Cline, M. V. Diwan, B. Fleming, M. Goodman and Z. J. Hladysz *et al.*, arXiv:0907.4183 [hep-ex].

[37] K. Scholberg, arXiv:astro-ph/0701081.

[38] A. Dighe, arXiv:0809.2977 [hep-ph].

[39] D. Barker, D. M. Mei and C. Zhang, arXiv:1202.5000 [physics.ins-det].